Slow Fluid Antenna Multiple Access

Kai-Kit Wong, *Fellow, IEEE,* David Morales-Jimenez, *Senior Member, IEEE,*
Kin-Fai Tong, *Fellow, IEEE,* and Chan-Byoung Chae, *Fellow, IEEE*

***Abstract*—Fluid antennas offer a novel way to achieve massive connectivity by enabling each user to find a 'port' in space where the instantaneous interference undergoes a deep null for multiple access. While this unprecedented capability permits hundreds of users to share the same radio channel, each user needs to switch its best port on a symbol-by-symbol basis, which is impractical. Motivated by this, this paper considers the scenario in which the fluid antenna of each user updates its best port only if the fading channel changes. We refer to this approach as *slow* fluid antenna multiple access (s-FAMA). In this paper, we first investigate the interference immunity of s-FAMA through analyzing the outage probability. Then an outage probability upper bound is obtained, from which we shed light on the achievable multiplexing gain of the system and unpack the impacts of various system parameters on the performance. Numerical results reveal that despite having a weaker multiplexing power than the symbol-based, *fast* FAMA (i.e., f-FAMA), spatial multiplexing of 4 users or more is possible if the users' fluid antennas have large numbers of ports.**

***Index Terms*—Fluid antennas, Interference immunity, Massive connectivity, Multiple access, Outage probability.**

I. Introduction

One of the great promises that 5G and future mobile communications networks look to deliver is massive connectivity which is the backbone of a world with connected intelligence [1]. At present, the *de facto* mobile communication technology for realizing massive connectivity is massive multiple-input multiple-output (MIMO) [2] whereas non-orthogonal multiple access (NOMA) is also being sold as the technology for greater capacity by overlapping users on the same radio channel [3]. In 5G, the base station (BS) is equipped with 64 antennas to support 6 users per channel use by matched filter beamforming based on the channel state information (CSI) at the BS.[1] This BS-led solution, however, is inflexible and both hardware and software upgrades will be needed in the standard if more BS antennas are to be commissioned to increase capacity.

The work of K. Wong is supported by the Engineering and Physical Sciences Research Council (EPSRC) under grant EP/W026813/1. For the purpose of open access, the authors will apply a Creative Commons Attribution (CC BY) licence to any Author Accepted Manuscript version arising.

The work of D. Morales-Jimenez is supported in part by the State Research Agency (AEI) of Spain and the European Social Fund under grant RYC2020-030536-I and by AEI under grant PID2020-118139RB-I00.

The work of C. B. Chae is partly supported by the IITP grant funded by the Korean government (MSIT) (No. 2021-0-02208, No. 2021-0-00486).

K. K. Wong and K. F. Tong are with the Department of Electronic and Electrical Engineering, University College London, London WC1E 7JE, UK. K. K. Wong is also affiliated with Yonsei University, Seoul, Korea.

D. Morales-Jimenez is with the Department of Signal Theory, Networking and Communications, University of Granada, Granada 18071, Spain.

C.-B. Chae is with School of Integrated Technology, Yonsei University, Seoul, Korea.

[1]Evidently, multiuser MIMO with 64 antennas at the transmitter can support 64 users (or more) but this requires more sophisticated precoding, e.g., dirty-paper coding. By contrast, an excessive number of BS antennas is considered for massive MIMO so that a relatively simple precoder can be used.

On the other hand, the high capacity of NOMA comes with the requirement of performing multiuser power control, user clustering and successive interference cancellation (SIC) at the users. The use of SIC at each user imposes decoding complexity and delay while the power control and user clustering require the BS to possess the CSI. Needless to say, NOMA is an 'expensive' technique, more so if more users are involved. For this reason, the majority of literature only focused on two-user NOMA where the complexity can be affordable.

To summarize, the state-of-the-art multiple access technologies such as massive MIMO and NOMA require tremendous efforts at the BS to acquire the full CSI and then optimize its transmission with the aid of CSI and with NOMA, also need multiuser detection to tackle the inter-user interference at each user. Looking ahead, it is of great interest to study if massive multiple access can be accomplished without the need of heavy processing at the BS, nor multiuser detection. The goal of this paper is to investigate a radical multiple access approach that does not require precoding at the BS nor multiuser detection at the users, yet allowing several users to share the same time-frequency channel towards massive connectivity.

A. Multiple Access via Fluid Antenna

Recently in [4], Wong *et al.* advocated that multiple access can be achieved by exploiting the ups and downs of the fading envelopes of the interference signals using the emerging fluid antenna technology. In particular, a software-controlled, port-switcheable antenna empowers a user the ability to tune in to the window of opportunity in which the interference naturally disappears in a deep fade. Fluid antenna refers to any software-controllable fluidic, conductive or dielectric radiating structure that can change their shape and/or position to reconfigure the operating frequency, radiation pattern and other characteristics. They can be realized by liquid-based radiating structures [5], [6] or reconfigurable pixels [7]–[9]. Single-user fluid antenna systems have been investigated in [10]–[16] where promising performance was revealed. An overview paper which covers different aspects of fluid antenna can be found in [17].

For multiuser communications in the downlink, the received signal at the k-th port of fluid antenna for user u is given by

$$r_k^{(u)} = s_u g_k^{(u,u)} + \underbrace{\sum_{\substack{\tilde{u}=1 \\ \tilde{u}\neq u}}^{U} s_{\tilde{u}} g_k^{(\tilde{u},u)} + \eta_k^{(u)}}_{\tilde{g}_k^{(u)}}, \tag{1}$$

where s_u denotes the transmitted symbol for user u, $\eta_k^{(u)}$ is the zero-mean complex additive white Gaussian noise (AWGN) at the k-th port for user u, $g_k^{(\tilde{u},u)}$ denotes the fading channel from

the BS antenna dedicated for transmitting user $\tilde{u}$'s signal to the k-th port of user u, and $\tilde{g}_k^{(u)}$ denotes the overall interference plus noise signal at a symbol instant. In this model, each BS antenna is assigned to transmit the signal for a given user in the downlink. In [4], it was proposed to find:

$$k_u^{f\text{-FAMA}} = \arg\max_k \frac{\left|g_k^{(u,u)}\right|^2}{\left|\tilde{g}_k^{(u)}\right|^2}. \tag{2}$$

That is, each user should select the port such that the symbol-level signal energy to the interference energy is maximized for multiple access. It was reported in [4], [18] that hundreds of users can be accommodated on the same time-frequency radio channel, all by a single RF-chain fluid antenna at each user without precoding at the BS nor multiuser detection at the users. Nonetheless, (2) requires port switching on a symbol-by-symbol basis which is extremely difficult to achieve. Even though reconfigurable pixels-based fluid antennas could switch ports without delay and recent work also addressed how the ratios (2) at the ports could be estimated for each symbol [19], there was still the complexity of observing a large number of signals (equalling the number of ports) at each symbol instant, which could be impractical. In [17], this approach is referred to as fast fluid antenna multiple access (f-FAMA).

Knowing the difficulty of f-FAMA, this paper hence considers a more practical scenario where the fluid antennas at the users only update their ports if the fading channels change. In other words, the selected ports for the users remain unchanged until the fading channels change. In this case, we have

$$k_u^{s\text{-FAMA}} = \arg\max_k \frac{\left|g_k^{(u,u)}\right|^2}{\sum_{\substack{\tilde{u}=1\\ \tilde{u}\neq u}}^{U}\left|g_k^{(\tilde{u},u)}\right|^2}, \tag{3}$$

in which $\mathrm{E}[|s_u|^2] = \sigma_s^2\ \forall u$ (hence cancelled in the ratios) and the noise power is dropped because the system performance is interference-limited. This is particularly true if the number of users, U, is large.[2] This approach (3) is referred to as slow fluid antenna multiple access (s-FAMA) which is more realistic than f-FAMA. For s-FAMA, not only do the ports change slowly, the average signal-to-interference ratio (SIR) at each port can also be estimated easily using standard methods.

Comparing (2) and (3), it is clear that the information symbols of the users help create the nulls of the sum-interference in the f-FAMA case while s-FAMA needs to find a region of space where the fading envelopes of the interferers all fall at the same time. The concept of s-FAMA is illustrated in Fig. 1 in which a 3-user downlink network is considered. Apparently, the opportunity s-FAMA exploits is certainly more restrictive and will impact the interference immunity at each user.

Motivated by the practicality of s-FAMA and different from [4], this paper aims to understand the achievable performance of s-FAMA. To simplify our discussion,[3] each user is assumed to have an N-port fluid antenna of size $W\lambda$ where λ is the wavelength and that all the users are statistically identical. A port refers to a physical location at which the fluid antenna can be switched to instantly. Each user always selects its port according to (3). Our contributions include a number of theoretical results for characterizing the fundamental performance of s-FAMA. First, we derive the outage probability of a typical user given an SIR target, γ, and then an outage probability upper bound is found to shed light on the interference immunity of s-FAMA. Also, through a lower bound, we reveal how the network capacity scales with N, γ, U and W. While [4] analyzed the performance of f-FAMA under rich scattering channels, s-FAMA is much less known, with the only work in [20] studying the performance of s-FAMA in millimeter-wave channels using computer simulations. Different from [20], this paper focuses on rich scattering channels and aims to analytically characterize the outage probability and multiplexing gain performance of s-FAMA, which has not been done before.

B. Summary of Results

Before proceeding to the main body of this paper, we here state some of our principal results. This summary aims to give the reader an overall view of the material covered in this paper and highlight our key findings for s-FAMA systems.

- For $W \geq 1$, the outage probability for a user, with an SIR target γ, is upper bounded by

$$\mathrm{Prob}(\mathrm{SIR} < \gamma) < \left[1 - N\left(\frac{1-\frac{1}{\pi W}}{\gamma}\right)^{U-1}\right]^+,$$[4]

  where $(a)^+ = \max\{0, a\}$. This result illustrates how the interference immunity depends on the parameters N, γ, U and W. It can be seen that N and W help bring down the outage probability while both U and γ play major roles in increasing the outage probability. For supporting more users U or more ambitious γ, N will need to be increased a lot to counter the rise in the outage probability.
- The multiplexing gain, m, is bounded by

$$U \geq m \geq \min\left\{NU\left(\frac{1-\frac{1}{\pi W}}{\gamma}\right)^{U-1}, U\right\}.$$

  Like in f-FAMA, the multiplexing gain, m, for s-FAMA also scales linearly with the number of ports, N, but is inversely proportional to the $(U-1)$-th power of the SIR target, γ. The size W also affects the capacity scaling but its impact is less significant if W is not too small.

The rest of the paper is organized as follows. In Section II, we introduce the network model of s-FAMA in the downlink. Our main results will be presented in Section III. Section IV provides the numerical results that illustrate the performance of s-FAMA. Finally, we conclude this paper in Section V.

[2]The mathematical analysis in this paper will be based on the interference-limited assumption where noise is ignored. However, the presence of noise will be considered in some of the numerical results for validation.

[3]If the users are not statistically identical, and/or their fluid antennas are of different sizes, the analysis can still be conducted but gaining insight would be more difficult. Therefore, we opt for the homogeneous user setup.

[4]This bound is based on some approximations which will be accurate if γ and W are large. More details will be provided when the result is derived.

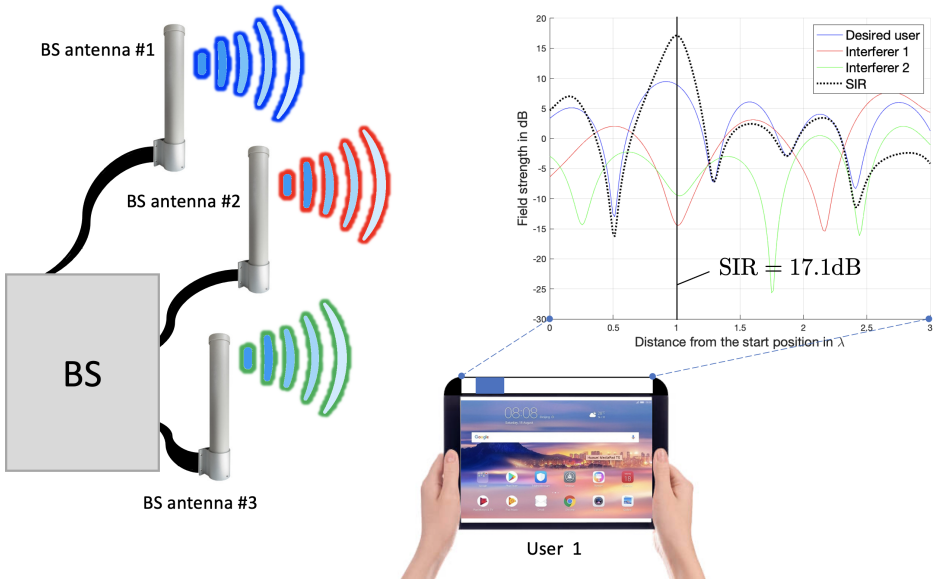

Fig. 1. The concept of s-FAMA for a 3-user network in the downlink where each BS antenna is assigned to transmit one user's signal and it is illustrated that user 1 can use its fluid antenna to tune in to the space where the fading envelopes of the other users are in a deep fade.

II. Downlink s-FAMA

A downlink of U mobile users served by a U-antenna BS is considered. Each BS antenna is dedicated to transmitting one user's signal. The BS antennas are distributed far apart so that their channels to a given user appear completely independent.[5] Each user is equipped with an N-port fluid antenna which is assumed to always switch to its best port for maximizing the SIR, as in (3). The port selection for user u is aimed at

$$k_u^{s\text{-FAMA}} = \arg\max_k \frac{\mathrm{E}\left[\left|g_k^{(u,u)} s_u\right|^2\right]}{\mathrm{E}\left[\left|\sum_{\substack{\tilde{u}=1 \\ \tilde{u}\neq u}}^{U} g_k^{(\tilde{u},u)} s_{\tilde{u}}\right|^2\right]} = \arg\max_k \frac{\left|g_k^{(u,u)}\right|^2}{\sum_{\substack{\tilde{u}=1 \\ \tilde{u}\neq u}}^{U} \left|g_k^{(\tilde{u},u)}\right|^2}, \quad (4)$$

where the variables have been defined in (1).

The amplitude of the channel, $|g_k^{(\tilde{u},u)}|$, is assumed Rayleigh distributed, with the probability density function (pdf)

$$p_{\left|g_k^{(\tilde{u},u)}\right|}(r) = re^{-\frac{r^2}{\sigma^2}}, \text{ for } r \geq 0 \text{ with } \mathrm{E}[|g_k^{(\tilde{u},u)}|^2] = 2. \quad (5)$$

The average received signal-to-noise ratio (SNR) at each port is given by $\Gamma = \frac{2\sigma_s^2}{\sigma_\eta^2}$ where $\sigma_s^2 = \mathrm{E}[|s_u|^2]$ and σ_η^2 is the noise power. The channels $\{g_k^{(\tilde{u},u)}\}_{\forall k}$ are considered to be correlated as they can be arbitrarily close to each other. To model the correlation between the channels at the ports, we parameterize $g_k^{(\tilde{u},u)}$, through a single correlation parameter μ, as

$$g_k^{(\tilde{u},u)} = \left(\sqrt{1-\mu^2} x_k^{(\tilde{u},u)} + \mu x_0^{(\tilde{u},u)}\right) + j\left(\sqrt{1-\mu^2} y_k^{(\tilde{u},u)} + \mu y_0^{(\tilde{u},u)}\right), \ k = 1, \ldots, N, \quad (6)$$

[5]Spatial correlation between BS antennas will be considered in the numerical results in Section IV.

where $x_0^{(\tilde{u},u)}, \ldots, x_N^{(\tilde{u},u)}, y_0^{(\tilde{u},u)}, \ldots, y_N^{(\tilde{u},u)}$ are all independent Gaussian random variables with zero mean and variance of 1. Using this model, the correlation among the ports is realized through the common random variables $x_0^{(\tilde{u},u)}$ and $y_0^{(\tilde{u},u)}$. To help model the spatial correlation between any two ports, we follow the approach in [18] and set

$$\mu = \sqrt{2}\sqrt{{}_1F_2\left(\frac{1}{2}; 1, \frac{3}{2}; -\pi^2 W^2\right) - \frac{J_1(2\pi W)}{2\pi W}}, \quad (7)$$

where ${}_aF_b(\cdot;\cdot;\cdot)$ denotes the generalized hypergeometric function and $J_1(\cdot)$ is the first-order Bessel function of the first kind. Setting μ using (7) allows all the ports to be correlated with each other and achieves the same mean correlation coefficient for an N-port linear structure of length $W\lambda$ [18, Theorem 1]. According to [18, Theorem 2], μ can be approximated as

$$\mu \approx \begin{cases} 1 - \dfrac{\pi^2 W^2}{12}, & \text{for } W \leq 0.6, \\ \dfrac{1}{\sqrt{\pi W}}, & \text{for } W \geq 1. \end{cases} \quad (8)$$

The above approximation will be useful to link the achievable performance of s-FAMA to the size of the fluid antenna in the subsequent analysis. In this paper, we focus on $W \geq 1$ since it corresponds to the typical size of a handset in the 5G bands.

Note that if we consider the distance between each user and the BS, the users should have different path loss. However, normally, power control would be used to obtain just enough received power at the user for a given required performance. In other words, power control has an effect of cancelling the path loss. With perfect power control, the system is as if the users are all independent and identically distributed (i.i.d.) and path loss does not exist. In what follows, we model, without loss of generality, that all users are i.i.d. from the BS and that BS antenna u is assigned to transmit to user u without path loss, which is the model we adopt in this paper.

For the s-FAMA downlink system, starting with the model in (1), we can write the signal-to-interference plus noise ratio (SINR) at port k as

$$\mathrm{SINR}_k = \frac{\mathrm{E}\left[\left|s_u g_k^{(u,u)}\right|^2\right]}{\mathrm{E}\left[\left|\sum_{\tilde{u}\neq u} s_{\tilde{u}} g_k^{(\tilde{u},u)} + \eta_k^{(u)}\right|^2\right]}, \tag{9}$$

which can be simplified as

$$\mathrm{SINR}_k = \frac{\left|g_k^{(u,u)}\right|^2 \mathrm{E}\left[|s_u|^2\right]}{\mathrm{E}\left[\left|\sum_{\tilde{u}\neq u} s_{\tilde{u}} g_k^{(\tilde{u},u)}\right|^2\right] + \sigma_\eta^2} \tag{10}$$

$$= \frac{\sigma_s^2 \left|g_k^{(u,u)}\right|^2}{\sigma_s^2 \sum_{\tilde{u}\neq u} \left|g_k^{(\tilde{u},u)}\right|^2 + \sigma_\eta^2}. \tag{11}$$

After ignoring the noise power in the denominator, we then have the SIR at port k given by

$$\mathrm{SIR}_k = \frac{\left|g_k^{(u,u)}\right|^2}{\sum_{\tilde{u}\neq u} \left|g_k^{(\tilde{u},u)}\right|^2}. \tag{12}$$

As a result, with the fluid antenna operating to maximize the SIR over all the ports, for user u, we have

$$\mathrm{SIR} = \max_k \frac{\left|g_k^{(u,u)}\right|^2}{\sum_{\substack{\tilde{u}=1\\ \tilde{u}\neq u}}^{U} \left|g_k^{(\tilde{u},u)}\right|^2} = \max_k \frac{\left|\frac{g_k^{(u,u)}}{\sqrt{1-\mu^2}}\right|^2}{\sum_{\substack{\tilde{u}=1\\ \tilde{u}\neq u}}^{U} \left|\frac{g_k^{(\tilde{u},u)}}{\sqrt{1-\mu^2}}\right|^2} \equiv \max_k \frac{X_k}{Y_k}, \tag{13}$$

where

$$X_k = \left(x_k^{(u,u)} + \frac{\mu}{\sqrt{1-\mu^2}} x_0^{(u,u)}\right)^2 + \left(y_k^{(u,u)} + \frac{\mu}{\sqrt{1-\mu^2}} y_0^{(u,u)}\right)^2 \tag{14}$$

and

$$Y_k = \sum_{\substack{\tilde{u}=1\\ \tilde{u}\neq u}}^{U} \left[\left(x_k^{(\tilde{u},u)} + \frac{\mu}{\sqrt{1-\mu^2}} x_0^{(\tilde{u},u)}\right)^2 + \left(y_k^{(\tilde{u},u)} + \frac{\mu}{\sqrt{1-\mu^2}} y_0^{(\tilde{u},u)}\right)^2\right]. \tag{15}$$

Our objective is to study the outage probability

$$\mathrm{Prob}\left(\mathrm{SIR} = \max_k \frac{X_k}{Y_k} < \gamma\right). \tag{16}$$

Our aim is to unpack the impact of different parameters on the various system performance. Note that a key difference from [4] is that the interference term in [4] is Rayleigh distributed while Y_k in this paper is Chi-squared distributed, which makes the outage probability analysis so much more challenging.

III. Main Results

In this section, we present our principal results that characterize the performance of s-FAMA systems. The first result is an SIR-based outage probability expression which reveals the interference immunity of each user. Then an upper bound for the outage probability is derived to help illustrate the impact of the different system parameters. Capacity scaling of s-FAMA in terms of multiplexing gain will also be analyzed. The results will be presented as theorems and corollaries, each of which presents a new analytical result and the next result is often a natural progression of the previous one. The results also tend to be mathematical but are the main contributions of this paper.

Theorem 1: The integral

$$\mathcal{I} = \int_0^\infty Q_1(c, \sqrt{\gamma}\beta) \left(\frac{\beta}{a}\right)^{M-1} \beta e^{-\frac{\beta^2+a^2}{2}} I_{M-1}(a\beta) d\beta, \tag{17}$$

where $I_k(\cdot)$ is the modified Bessel function of the first kind, and $Q_m(\cdot,\cdot)$ denotes the generalized Marcum-Q function, has the closed-form expression (18) (see top of next page) where $(a)_j$ represents the Pochhammer symbol.

Proof: See Appendix A. ∎

Corollary 1: Letting $b = a^2$, $\mathcal{I}$ can be rewritten as

$$\mathcal{I} = \frac{1}{2} \int_0^\infty Q_1(c, \sqrt{\gamma y}) \left(\frac{y}{b}\right)^{\frac{M-1}{2}} e^{-\frac{y+b}{2}} I_{M-1}(\sqrt{by}) dy, \tag{19}$$

which can then be expressed as (20) (see next page).

Proof: The result can be obtained by using the substitution $b = a^2$ and changing the variable $\beta^2 = y$ in (17) and then applying (18), which completes the proof. ∎

Theorem 2: The outage probability for an s-FAMA user with an SIR threshold, γ, is given by (21) (see next page), in which $\Gamma(n) = (n-1)!$ is the gamma function.

Proof: See Appendix B. ∎

Note that as $z \to \infty$, $I_{j+k}(z) \to \infty$ and the expression in (21) can be problematic in numerical computation. To address this, the following corollary provides an alternative expression.

Corollary 2: The outage probability for an s-FAMA user in (21) can be expressed as (22) (see next page).

Proof: See Appendix C. ∎

Theorem 3: The SIR outage probability expression in (21) is upper bounded by[6]

$$\mathrm{Prob}\left(\mathrm{SIR} < \gamma\right) < \left[1 - N\left(\frac{\mu^2}{\gamma+1}\right)^{U-1} - N\left(\frac{1-\mu^2}{\gamma}\right)^{U-1}\right]^+, \tag{23}$$

which for small μ and large γ can be simplified as

$$\mathrm{Prob}\left(\mathrm{SIR} < \gamma\right) < \left[1 - N\left(\frac{1-\mu^2}{\gamma}\right)^{U-1}\right]^+. \tag{24}$$

[6]It is worth noting that the results are based on linearization in N and the operation $(\cdot)^+$ is to ensure that the bound is never negative. In particular, the result comes from a sequence of approximations and the conditions under which the bound is accurate will be discussed at the end of Appendix D.

$$\mathcal{I} = 1 - Q_M\left(a\sqrt{\frac{\gamma}{1+\gamma}}, c\sqrt{\frac{1}{1+\gamma}}\right) + \left(\frac{1}{1+\gamma}\right)^M \exp\left[\frac{a^2}{2}\left(\frac{1}{1+\gamma}-1\right) - \frac{c^2}{2(1+\gamma)}\right] \times \sum_{k=0}^{M-1}\sum_{j=0}^{M-k-1} \frac{(M-k-j)_j}{j!}\left(\frac{c}{a}\right)^{j+k}(1+\gamma)^k(\sqrt{\gamma})^{j-k} I_{k+j}\left(\frac{ac\sqrt{\gamma}}{1+\gamma}\right) \quad (18)$$

$$\mathcal{I} = 1 - Q_M\left(\sqrt{b}\sqrt{\frac{\gamma}{1+\gamma}}, c\sqrt{\frac{1}{1+\gamma}}\right) + \left(\frac{1}{1+\gamma}\right)^M e^{-\frac{1}{2(\gamma+1)}(b\gamma+c^2)} \sum_{k=0}^{M-1}\sum_{j=0}^{M-k-1} \frac{(M-k-j)_j}{j!}\left(\frac{c}{\sqrt{b}}\right)^{j+k}(1+\gamma)^k(\sqrt{\gamma})^{j-k} I_{k+j}\left(\frac{c\sqrt{\gamma b}}{1+\gamma}\right) \quad (20)$$

$$\text{Prob}\left(\text{SIR} < \gamma\right) = \int_0^\infty \int_0^\infty \frac{\tilde{r}^{U-2}}{2^U\Gamma(U-1)} e^{-\frac{r+\tilde{r}}{2}} \left\{ Q_{U-1}\left(\frac{\mu}{\sqrt{1-\mu^2}}\sqrt{\frac{\gamma\tilde{r}}{\gamma+1}}, \frac{\mu}{\sqrt{1-\mu^2}}\sqrt{\frac{r}{\gamma+1}}\right) - \left(\frac{1}{\gamma+1}\right)^{U-1} e^{-\frac{\mu^2}{2(1-\mu^2)}\left(\frac{\gamma\tilde{r}+r}{\gamma+1}\right)} \times \sum_{k=0}^{U-2}\sum_{j=0}^{U-k-2} \frac{(U-(j+k)-1)_j}{j!}\left(\frac{r}{\tilde{r}}\right)^{\frac{j+k}{2}}(\gamma+1)^k\gamma^{\frac{j-k}{2}} I_{j+k}\left(\frac{\mu^2}{1-\mu^2}\frac{\sqrt{\gamma r\tilde{r}}}{(\gamma+1)}\right)\right\}^N dr d\tilde{r}, \quad (21)$$

$$\text{Prob}\left(\text{SIR} < \gamma\right) = \int_0^\infty \int_0^\infty \frac{\tilde{r}^{U-2}}{2^U\Gamma(U-1)} e^{-\frac{r+\tilde{r}}{2}} \left\{ Q_{U-1}\left(\frac{\mu}{\sqrt{1-\mu^2}}\sqrt{\frac{\gamma\tilde{r}}{\gamma+1}}, \frac{\mu}{\sqrt{1-\mu^2}}\sqrt{\frac{r}{\gamma+1}}\right) - \frac{1}{\pi}\left(\frac{1}{\gamma+1}\right)^{U-1} e^{-\frac{\mu^2}{2(1-\mu^2)}\frac{1}{\gamma+1}\left(\sqrt{\gamma\tilde{r}}-\sqrt{r}\right)^2} \times \sum_{k=0}^{U-2}\sum_{j=0}^{U-k-2} \frac{(U-(j+k)-1)_j}{j!}\left(\frac{r}{\tilde{r}}\right)^{\frac{j+k}{2}}(\gamma+1)^k\gamma^{\frac{j-k}{2}} \int_0^\pi \cos\left((j+k)\theta\right) e^{-\frac{\mu^2}{1-\mu^2}\left(\frac{1}{\gamma+1}\right)\sqrt{\gamma\tilde{r}r}(1-\cos\theta)} d\theta\right\}^N dr d\tilde{r}, \quad (22)$$

For $W \geq 1$, the upper bound can further be written as

$$\text{Prob}\left(\text{SIR} < \gamma\right) < \left[1 - N\left(\frac{1-\frac{1}{\pi W}}{\gamma}\right)^{U-1}\right]^+. \quad (25)$$

Proof: See Appendix D. ∎

Corollary 3: As $N \to \infty$, the outage probability goes to 0.

Proof: This can be directly observed from (25). ∎

Corollary 3 confirms that if N is allowed to be very large, then the outage probability for an s-FAMA user can be made arbitrarily small. However, the conclusion may be different if the channel model is different. In [20], it was reported that there was an irreducible outage probability floor even if N was to increase without bound when a multi-ray channel model was used. The discrepancies will be discussed in Section IV.

In the following, several insightful results will be derived using the expression (25) by ignoring the $(\cdot)^+$ operation. This will be valid if N is not too large and the outage probability behaves as a linear function of N. Otherwise, this implies that the outage probability is already very close to zero.

Corollary 4: To maintain the same protection at each user from the interference while supporting Δ additional users, the number of ports for an s-FAMA user should be increased to

$$N' = N\left(\frac{\gamma}{1-\frac{1}{\pi W}}\right)^{\Delta}. \quad (26)$$

Proof: Consider two cases, one with N ports and U users and another with N' ports and $U+\Delta$ users and then set the outage probability bound (25) for the two cases to be the same. Then (26) is obtained, which completes the proof. ∎

As in [4], we can evaluate the average outage rate of the s-FAMA network using

$$C(\gamma) = U(1 - \text{Prob}\left(\text{SIR} < \gamma\right))\log_2(1+\gamma). \quad (27)$$

This corresponds to the case in which the BS transmits a fixed coding rate to the users and therefore, the achievable rate for each user is discounted by the outage probability.

Theorem 4: The multiplexing gain of the s-FAMA network,

m, is bounded by

$$U \geq m \geq \min\left\{NU\left(\frac{1-\frac{1}{\pi W}}{\gamma}\right)^{U-1}, U\right\}. \quad (28)$$

Proof: First, the multiplexing gain is the capacity scaling factor given by

$$m = \frac{C(\gamma)}{\log_2(1+\gamma)} = U(1-\text{Prob}\left(\text{SIR} < \gamma\right)), \quad (29)$$

which is upper bounded by U. Note that if users are overlapped on the same radio channel with interference cancellation, their outage probability will be close to one and $m \approx 0$. The use of fluid antennas at the users serves to avoid the interference and decrease the outage probability to an acceptable level if N is sufficiently large. For the lower bound of m in (28), this can be directly obtained by substituting the outage probability upper bound (25) in (29), and recognizing that $m \leq U$ ■

The multiplexing gain lower bound in (28) reveals clearly how the network capacity scales with the parameters N, γ, W and U. If W is reasonably large, then $\left(1-\frac{1}{\pi W}\right)^{U-1} \approx 1$ and the multiplexing gain lower bound becomes

$$m \gtrsim \frac{NU}{\gamma^{U-1}}. \quad (30)$$

It can be estimated that if the network needs to achieve the maximum multiplexing gain of U, then $N = \gamma^{U-1}$. Evidently, if W is small, then the required N will be much larger.

Definition 1: We can define the multiplexing efficiency, η, of s-FAMA, which measures the rate of increase in m/U with respect to (w.r.t.) N in the linear region of m/U (i.e., when m/U is a linear function of N), by[7]

$$\eta \triangleq \left(\frac{m}{U}\right)\frac{1}{N} = \left(\frac{1-\frac{1}{\pi W}}{\gamma}\right)^{U-1}. \quad (31)$$

From the above definition, we can estimate that if $W = 1$ and $\gamma = 1$, then $1 - \frac{1}{\pi W} \approx 0.68$ and η becomes

$$\eta \doteq (0.68)^{U-1} \quad (32)$$

which is 46% if $U = 3$ users are supported, and is reduced to 31% if U is increased to 4 users. Clearly, it gets harder to protect the users if the number of users increases. In addition, as observed in (31), increasing γ (even by a little) will greatly penalize the efficiency, to the $(U-1)$-th power of γ. In other words, it would be more efficient to support more users with a less SIR target than less users with a harsher SIR target.

Corollary 5: The s-FAMA system can support Δ additional users to maintain the same overall multiplexing gain if the SIR target can be adjusted to γ' so that

$$\gamma' = \left(1+\frac{\Delta}{U}\right)^{\frac{1}{U-1+\Delta}}\left(1-\frac{1}{\pi W}\right)^{\frac{\Delta}{U-1+\Delta}}\gamma^{\frac{U-1}{U-1+\Delta}}. \quad (33)$$

Proof: Using the lower bound in (28) as an estimate of the multiplexing gain, we require

$$NU\left(\frac{1-\frac{1}{\pi W}}{\gamma}\right)^{U-1} = N(U+\Delta)\left(\frac{1-\frac{1}{\pi W}}{\gamma'}\right)^{U-1+\Delta}, \quad (34)$$

which after manipulations will give the result (33). ■

Corollary 6: To achieve the same multiplexing gain lower bound, an s-FAMA network accommodating K times more users (i.e., KU users) will require to set their SIR target, γ', as the K-th root of the original SIR target γ. That is,

$$\gamma' \approx \gamma^{\frac{U-1}{KU-1}} \approx \sqrt[K]{\gamma}. \quad (35)$$

Proof: Substituting $\Delta = (K-1)U$ in (33) and recognizing that $\left(1+\frac{\Delta}{U}\right)^{\frac{1}{KU-1}} \approx 1$ and $\left(1-\frac{1}{\pi W}\right)^{\frac{\Delta}{KU-1}} \approx 1$, we obtain the approximation (35), which completes the proof. ■

Corollary 7: To maintain the same multiplexing gain lower bound while serving Δ more users, the number of ports for each user should be increased to

$$N' = \frac{N}{1+\frac{\Delta}{U}}\left(\frac{\gamma}{1-\frac{1}{\pi W}}\right)^{\Delta}. \quad (36)$$

Proof: The result is obtained if we set the multiplexing gain lower bound (28) for the two cases to be the same. ■

Corollary 8: For the s-FAMA network, there is no apparent capacity advantage of supporting more (less) users each with a less (more) SIR target. Letting $C_{s\text{-FAMA}}(\gamma)|_U$ be the average network outage rate lower bound of the s-FAMA network with U users each with a target SIR γ, it can be shown that it has roughly the same average network outage rate lower bound to serve U' users each with a target SIR $\gamma' = \sqrt[U']{\gamma^U}$, i.e.,

$$C_{s\text{-FAMA}}(\gamma)|_U \approx C_{s\text{-FAMA}}(\sqrt[U']{\gamma^U})\Big|_{U'}. \quad (37)$$

Proof: To show the result, we write

$$\begin{aligned} C_{s\text{-FAMA}}(\gamma)|_U &\overset{(a)}{=} UN\left(\frac{1-\frac{1}{\pi W}}{\gamma}\right)^{U-1}\log_2(1+\gamma) \\ &\overset{(b)}{\approx} \frac{UN}{\gamma^{U-1}}\log_2\gamma \\ &\overset{(c)}{=} \frac{U'N}{\gamma^{U-1}}\log_2\gamma^{\frac{U}{U'}} \\ &\overset{(d)}{\approx} \frac{U'N}{\gamma'^{U'-1}}\log_2\gamma' \\ &\overset{(e)}{\approx} C_{s\text{-FAMA}}(\sqrt[U']{\gamma^U})\Big|_{U'}, \end{aligned} \quad (38)$$

where (a) uses the definition of the average outage rate and the multiplexing gain lower bound (28), (b) approximates the expression when γ is large and W is small, (c) multiplies the expression with $\frac{U'}{U'}$ and then moves $\frac{U}{U'}$ inside the log, (d) uses the definition $\gamma' = \gamma^{\frac{U}{U'}}$ and (e) follows the definition of the average outage rate using the said approximations earlier. ■

IV. Numerical Results and Discussion

In this section, numerical results using the analytical results, (22) and (29), are provided to understand the performance of s-FAMA against various different parameters. We have assumed that all the users and channels are statistically identical and as in the analysis, noise is ignored. TABLE I lists the parameters and their values considered in the numerical evaluations.

[7]This definition differs from what is presented in [18] because m is a more complicated function of U and γ and a slight modification is thus needed.

TABLE I
SIMULATION PARAMETERS

Parameter	Value
Normalized size of fluid antenna, W	$0.1, 0.2, 0.5, 1, 2, 5$
Number of ports, N[§]	$10, 20, \ldots, 7000$
Target SIR, γ	$2, 4, 5, 6, 8, 10$
Number of s-FAMA users, U	$3, 4, 5, 6$

[§] For liquid-based fluid antennas [5], [6], the radiating element is usually moved using a digital pump and its resolution (i.e., the number of ports) is only limited by the number of bits controlling the pump. For example, if 10 bits are used, then a resolution of 1024 ports will be achieved. Furthermore, if 13 bits are used, then 8192 ports will be achieved. Even for reconfigurable pixel-based fluid antennas [7]–[9] that use an array of RF/MEMS on-off switches, the assumption of hundreds or even thousands of ports can be justifiable. For example, a typical mobile handset has dimensions of $160.8 \times 78.1 \times 7.7\text{mm}$, yet allowing a display resolution of up to 1284×2778 pixels. The future therefore is bright in allowing thousands of RF pixels (in a way similar to display pixels).

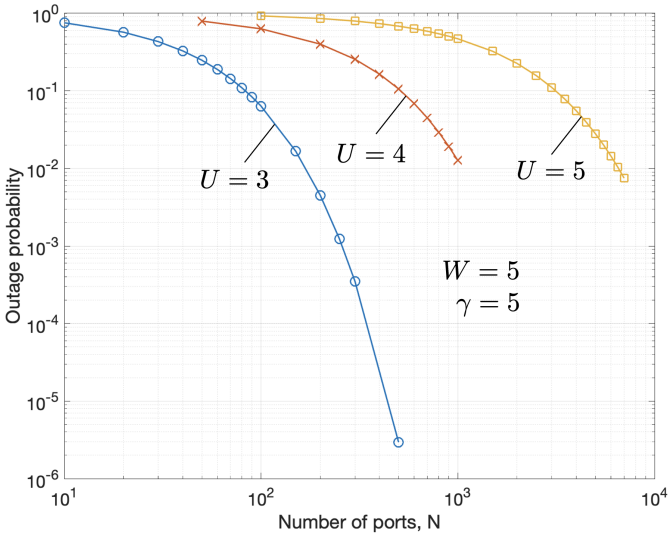

Fig. 2. The outage probability for s-FAMA against the number of ports, N, for different number of users, U, when $W = 5$ and $\gamma = 5$.

A. Main Observations

Fig. 2 demonstrates the outage probability results against the number of ports, N, at each user in s-FAMA systems with different number of users, U when the SIR threshold is $\gamma = 5$ and the size of each fluid antenna is 5λ (i.e., $W = 5$). The results indicate that the outage probability decreases when N increases as expected, as a fluid antenna with higher resolution has better ability to resolve the interference. In addition, it can be observed that if the number of users, U, increases, it will require so much larger N to keep the outage probability low. In particular, it appears that for a given U, the outage probability first decreases only very slowly as N increases. Nevertheless, when N reaches a certain number, the outage probability will begin to drop much more rapidly. Moreover, it appears that the outage probability can drop to any arbitrary value if N continues to increase, as predicted in Corollary 3.

The multiplexing gains of the same s-FAMA systems are illustrated in Fig. 3. As expected, the results indicate that the

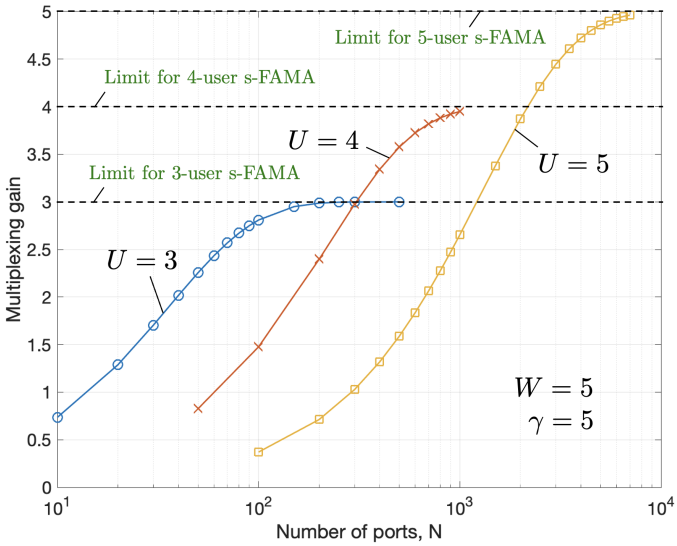

Fig. 3. The multiplexing gain for s-FAMA against the number of ports, N, for different number of users, U, when $W = 5$ and $\gamma = 5$.

multiplexing gain is a strictly increasing function of N while its maximum limit is the number of users, U. The results also reveal that with $U = 3$ users, we need $N = 200$ ports for the fluid antenna to achieve the maximum multiplexing gain. The required number is increased to $N = 1000$ ports to approach the maximum multiplexing gain if we have $U = 4$ users, and to $N = 7000$ ports for the case of $U = 5$ users. We can actually use the multiplexing gain lower bound in (28) to predict how many more ports are needed at the fluid antenna to achieve a given multiplexing gain if the number of users changes.

Consider two s-FAMA systems, one with U users and N ports and another with U' users and N' ports, both with the same W and γ. They achieve the same multiplexing gain if

$$NU\left(\frac{1-\frac{1}{\pi W}}{\gamma}\right)^{U-1} = N'U'\left(\frac{1-\frac{1}{\pi W}}{\gamma}\right)^{U'-1}, \quad (39)$$

which can be simplified to

$$\frac{N'}{N} = \frac{U}{U'}\left(\frac{\gamma}{1-\frac{1}{\pi W}}\right)^{U'-U}. \quad (40)$$

Therefore, with $W = 5$ and $\gamma = 5$, if we increase the number of users from 3 to 4, then $N'/N \approx 4$. Now, from Fig. 3, we see that $N = 40$ ports are needed to get the multiplexing gain of 2 if $U = 3$, and this number is increased to about $N = 160$ ports if $U = 4$, a four times increase in the number of ports, as predicted by (40). Furthermore, if U is increased to 5, (40) predicts that $N'/N \approx 15$ and the required number of ports to get the same multiplexing gain is 600 which is exactly what is observed in Fig. 3. These results confirm that the multiplexing gain lower bound (28) is accurate in characterizing the capacity scaling of s-FAMA as a function of the system parameters.

Another important parameter for the s-FAMA system is the size of fluid antenna, W, which we investigate using the results in Fig. 4. In this figure, results are provided for two configurations, $(U, \gamma, N) = (3, 5, 100)$ and $(U, \gamma, N) = (5, 5, 5000)$.

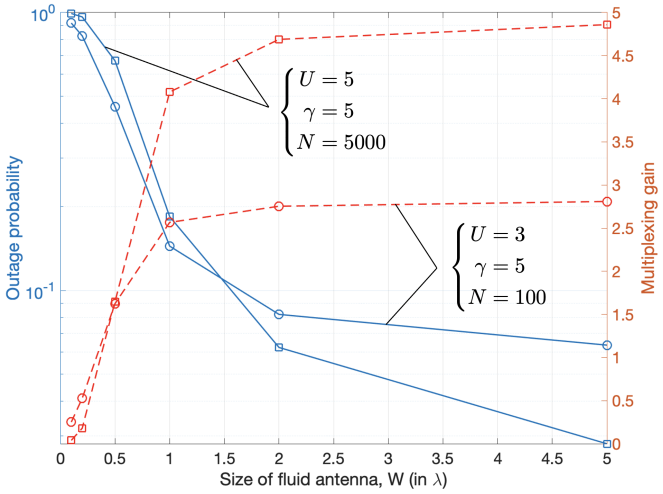

Fig. 4. The outage probability and multiplexing gain for s-FAMA against the size of fluid antenna, W when $\gamma = 5$.

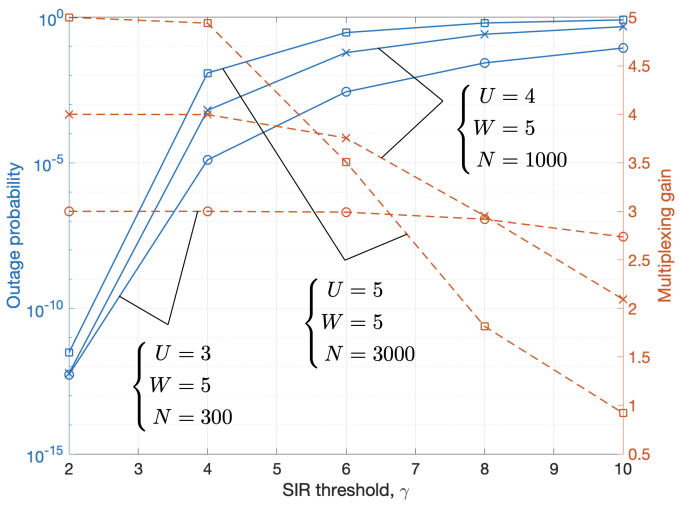

Fig. 5. The outage probability and multiplexing gain for s-FAMA against the SIR threshold, γ, for different U and N when $W = 5$.

The two configurations were selected because they had nearly the same outage probability performance if they have the same W, as seen in Fig. 2. Both outage probability and multiplexing gain results are examined. As can be observed, when W is really small, the outage probability will be unacceptably large and s-FAMA is not functioning and the multiplexing gain is nearly zero. The performance of s-FAMA however improves very quickly as W increases, faster when $W < 1$ than when $W > 1$. Therefore, $W = 1$ can be interpreted as the threshold size that one would expect to have in order for the s-FAMA system to work well. Also, $W = 2$ seems to be the required size for the two configurations to approach to the maximum multiplexing gain. On the other hand, we can rewrite the lower bound (28) and use it to estimate the required size for obtaining a given multiplexing gain m so that

$$W \approx \frac{1}{\pi}\left[1 - \gamma\left(\frac{m}{NU}\right)^{\frac{1}{U-1}}\right]^{-1}. \tag{41}$$

Using (41), we estimate that for $(U, \gamma, N) = (3, 5, 100)$, $W \approx 0.4475$ is required to yield $m = 1$. Also, for $m = 2$, $W \approx 0.5379$. Additionally, for $(U, \gamma, N) = (5, 5, 5000)$ and $m = 2$, $W \approx 0.6039$. These estimations agree with the results in Fig. 4. Note that (41) has used the approximation (8) for large W but surprisingly it works well in estimating small W.

Results in Fig. 5 are provided to examine the performance of s-FAMA when the SIR threshold, γ, changes. Three system configurations are considered and each considers a different number of users, U and has an appropriate number of ports, N, to have reasonable interference immunity. All have assumed that $W = 5$. Apparently, as γ increases, so does the outage probability and it does so very rapidly. This agrees with the observation we made from the outage probability upper bound (25) before. The results for the multiplexing gain reveal more about the impact of the value of γ on the system performance for different U. In particular, we can observe that with $U = 3$, the multiplexing gain decreases only very mildly when γ gets larger. However, the same cannot be said for the cases with $U = 4$ and $U = 5$, the latter of which suffers from a faster fall when γ increases. This is reasonable because (28) suggests that the multiplexing gain is inversely proportional to γ^{U-1}. Though the multiplexing gain is a decreasing function of γ, the overall network outage rate (27) is a more complex function of γ. We study the average network outage rates of the three configurations in Fig. 6. As we can see, for $U = 4$ and $U = 5$, the network rate first rises and then begins to fall as γ increases. This phenomenon can be seen analytically by observing the derivative of $C(\gamma)$ w.r.t. γ, i.e.,

$$\frac{\partial C(\gamma)}{\partial \gamma} = \begin{cases} D_1 \text{ for } \gamma \leq N^{\frac{1}{U-1}}\left(1 - \dfrac{1}{\pi W}\right), \\ D_2 \text{ otherwise,} \end{cases} \tag{42}$$

where $D_1 = \frac{U}{(\gamma+1)\ln 2}$ and

$$D_2 = -\frac{NU\left(1 - \frac{1}{\pi W}\right)^{U-1}\left[(\gamma+1)\ln(\gamma+1)^{U-1} - \gamma\right]}{\gamma^U(\gamma+1)\ln 2}. \tag{43}$$

Notice that $D_1 > 0$ and $D_2 < 0$, which shows that $C(\gamma)$ first increases and then decreases with γ, and that the maximum of $C(\gamma)$ occurs at

$$\gamma^* = N^{\frac{1}{U-1}}\left(1 - \frac{1}{\pi W}\right). \tag{44}$$

According to Fig. 6, however, (44) tends to overestimate the optimal SIR threshold, γ, in maximizing the network rate.

Besides, we have the results in Fig. 7 to investigate how the performance changes w.r.t. the number of users, U. Both the outage probability and multiplexing gain are shown and four configurations are considered for two different sizes, $W = 2, 5$, and two different numbers of ports, $N = 500, 3000$. The results in the figure illustrate, as expected, that as U increases, the outage probability rises for all configurations as it becomes harder to eliminate the interference. The results also indicate that the outage probability increases very fast as U increases. The results for multiplexing gain by contrast exhibit a more interesting trend. In particular, the multiplexing gain, m, first

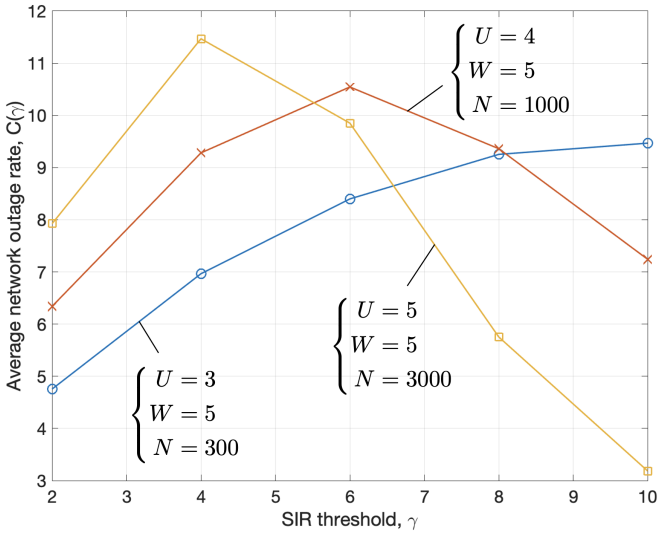

Fig. 6. The average network outage rate for s-FAMA against the SIR threshold, γ, for different U and N when $W = 5$.

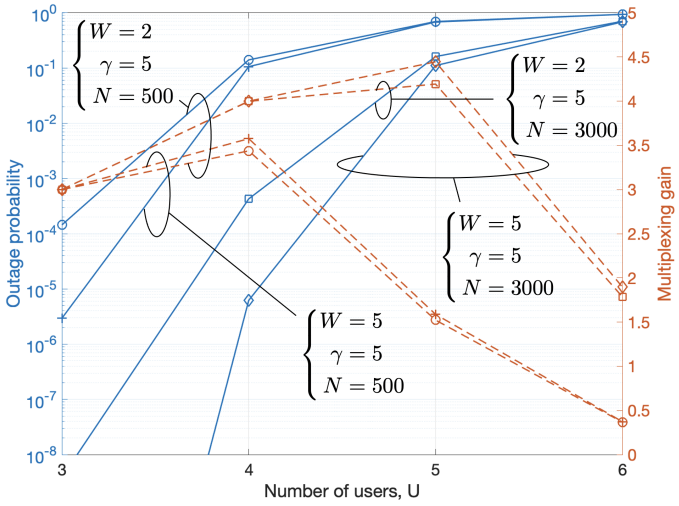

Fig. 7. The outage probability and multiplexing gain for s-FAMA against the number of users, U, for different W and N when $\gamma = 5$.

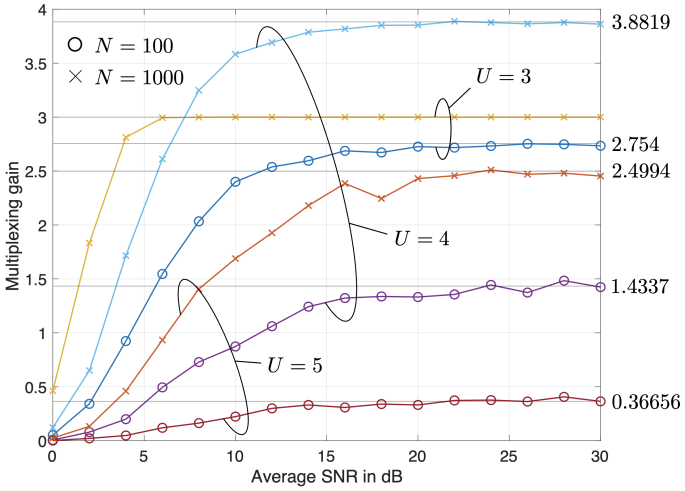

Fig. 8. The multiplexing gain performance for an U-user s-FAMA system against the average SNR when the SINR threshold is set to $\gamma = 5$ (or 7dB), and $W = 2$, with the number of ports, $N = 100$ or 1000.

increases with U and then drops when U continues to increase. The optimal number of users, U^*, in fact can be predicted by analyzing the derivative of m (or its lower bound (28)), i.e.,

$$\frac{\partial m}{\partial U} = \begin{cases} 1 \text{ for } N\left(\frac{1-\frac{1}{\pi W}}{\gamma}\right)^{U-1} \geq 1, \\ E \text{ otherwise,} \end{cases} \tag{45}$$

where

$$E = N\left(\frac{1-\frac{1}{\pi W}}{\gamma}\right)^{U-1}\left[U\ln\left(\frac{1-\frac{1}{\pi W}}{\gamma}\right)+1\right]. \tag{46}$$

It is easy to see that $E < 0$ and as a result, the turning point or maximum of m occurs at the boundary of the two intervals in (45) which then gives

$$U^* = \left\lfloor \frac{\ln N}{\ln\left(\frac{\gamma}{1-\frac{1}{\pi W}}\right)} + 1 \right\rfloor, \tag{47}$$

in which $\lfloor x \rfloor$ returns the largest integer less than or equal to x. Substituting the parameters of the configurations into (47) will estimate that for $(W, \gamma, N) = (2, 5, 500)$ and $(W, \gamma, N) = (5, 5, 500)$, $U^* = 4$ and for $(W, \gamma, N) = (2, 5, 3000)$ and $(W, \gamma, N) = (5, 5, 3000)$, $U^* = 5$. These estimates appear to match very well with the results in Fig. 7.

While our analysis is reliant on the no-noise assumption for mathematical tractability, we argue that in an s-FAMA system with several users sharing the same channel, the performance is dominated by the interference, rather than noise. This can be confirmed by the results in Fig. 8 when noise is present. The horizontal lines indicate the results predicted by Theorem 2. The detailed parameters of the simulations are described in the caption of the figure. As seen, the analytical result of Theorem 2 approaches that of the Monte-Carlo simulation results as the SNR increases. It is also observed that a higher SNR would be needed for the two results to coincide, if the number of users, U, is greater. However, an SNR of 20dB is quite enough for the no-noise assumption to be accurate. Additionally, the results indicate that the result of Theorem 2 gets more accurate, or is less sensitive to noise if N is larger provided the multiplexing gain has still not reached its maximum.

B. Trade-offs

There are indeed a few trade-offs in the s-FAMA network that are worth mentioning. First, the SINR threshold, γ, is a quality parameter at each user that can be chosen carefully to trade-off between individual and network performance. If γ is higher, then the expected performance of a user will be higher but with a given number of users, U, sharing the same spectrum, it will be more difficult or the outage probability will be higher. In terms of the overall network outage rate, as γ increases, each user's rate increases and if the fluid antenna is powerful enough to handle the interference (i.e., sufficient size, W, and number of ports, N), then the network outage rate

will increase. However, if γ becomes too large, then the outage probability will increase and suppress the network outage rate. That is why the network rate decreases when γ continues to increase without bound. This is the observation we have made from the results in Fig. 6. In fact, (44) provides an estimate of the optimal γ that maximizes the network outage rate.

On the other hand, there is also a trade-off between the number of users, U, and the multiplexing gain. With W and N fixed, if U is not too large, then each user's fluid antenna can still tolerate the interference, and the multiplexing gain will increase with U. As U continues to increase, each user will begin to suffer and the outage probability rises, thereby suppressing the multiplexing gain, as has been demonstrated in Fig. 7. Our result (47) estimating the optimal U for maximizing the multiplexing gain has also been confirmed.

Lastly, there is also a trade-off between the performance and complexity of the system. For improved performance, one can have each user using a fluid antenna with larger W and/or N which will mean higher complexity in implementation and signal processing. By increasing the number of ports at the fluid antenna of each user, this poses additional challenges for channel estimation. In theory, channel estimation is needed at every port of the fluid antenna at each user and if N is large, this will become infeasible, if not impossible. That said, recent studies have attempted to use deep learning to exploit the strong spatial correlation between the channel ports for low-complexity port selection so that channel estimation for only a few ports is sufficient to deliver near-optimal performance. The single-user case was addressed in [12] while the same was studied for s-FAMA systems recently in [21].

C. With Correlated BS Antennas

Here, we investigate the performance of s-FAMA if the BS antennas are correlated. In this case, a new channel model will be needed. To do so, we model the complex channel from the $\tilde{u}$-th BS antenna to the k-th port of user u as

$$g_k^{(\tilde{u},u)} = \epsilon\alpha_0^{(u)} + \sqrt{1-\epsilon^2}\left(\mu\beta_0^{(\tilde{u},u)} + \sqrt{1-\mu^2}\beta_k^{(\tilde{u},u)}\right), \tag{48}$$

in which $\alpha_0^{(u)}, \beta_0^{(\tilde{u},u)}, \beta_1^{(\tilde{u},u)}, \ldots, \beta_N^{(\tilde{u},u)}$ are all i.i.d. complex Gaussian random variables with zero mean and variance of 2. The parameter μ specifies the channel correlation across the antenna ports and should be set based on (7). Additionally, the common random variable $\alpha_0^{(u)}$ links all the channels over the BS antennas and the parameter $0 \leq \epsilon \leq 1$ controls the amount of spatial correlation between them. We provide the simulation results of the multiplexing gain for s-FAMA against the BS correlation parameter ϵ in Fig. 9. Several observations can be made. First of all, we can observe that as expected, if ϵ increases (i.e., when the correlation at the BS antennas becomes stronger), then the multiplexing gain drops in all the cases. Furthermore, the s-FAMA system is more robust to the BS antenna correlation if the number of ports, N, is larger. If the number of users, U, is not large, high correlation at the BS can be tolerated. For example, in the case of $N = 1000$, the s-FAMA system with $U = 3$ or $U = 4$ can still achieve high multiplexing gain even if ϵ is as large as 0.6. Finally, if U is too large and N is not large enough, then the multiplexing gain will be very small to start with and will not be too much affected by the correlation across the BS antennas.

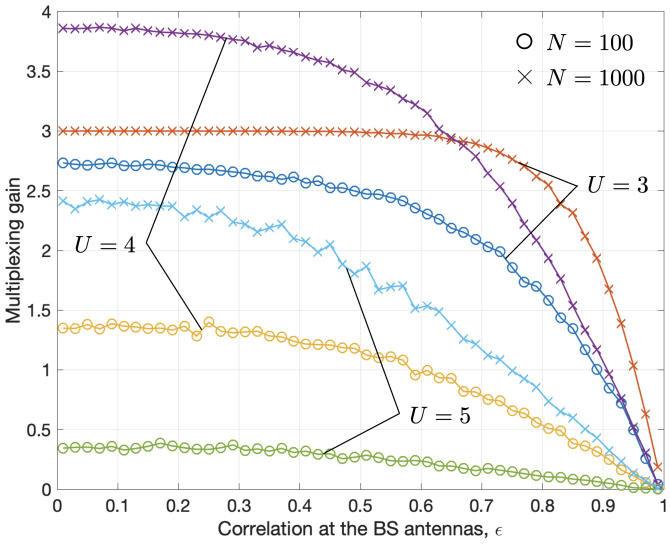

Fig. 9. The multiplexing gain performance for an U-user s-FAMA system against the correlation parameter, ϵ, at the BS antennas when the average SNR is 20dB, the SINR threshold is set to $\gamma = 5$ (or 7dB), and $W = 2$.

D. Discrepancies from Different Channel Model

Our performance analysis is based on the generalized channel correlation model by Beaulieu *et al.* in [22]. Evidently, there are other models. One emerging channel model which is popularly used for the millimeter-wave band is the multi-ray channel model [23], [24]. Using the multi-ray model, the channel between the $\tilde{u}$-th BS antenna and the k-th port of the fluid antenna at user u can be modelled as

$$g_k^{(\tilde{u},u)} = \sqrt{\frac{K\Omega}{K+1}} e^{j\alpha^{(\tilde{u},u)}} e^{-j\frac{2\pi(k-1)W}{N-1}\sin\theta_0^{(\tilde{u},u)}\cos\phi_0^{(\tilde{u},u)}} + \sum_{\ell=1}^{N_p} a_\ell^{(\tilde{u},u)} e^{-j\frac{2\pi(k-1)W}{N-1}\sin\theta_\ell^{(\tilde{u},u)}\cos\phi_\ell^{(\tilde{u},u)}}, \tag{49}$$

which consists of a specular component and N_p scattered components. For the specular component, it has an azimuth angle-of-arrival (AoA), θ_0, and an elevation AoA, ϕ_0, while the scattered components have the azimuth AoAs, $\{\theta_\ell\}_{\ell=1}^{N_p}$ and elevation AoAs, $\{\phi_\ell\}_{\ell=1}^{N_p}$. Also, K denotes the Rice factor (i.e., the power ratio between the specular and scattered components), Ω denotes the average power of the channel, $\alpha^{(\tilde{u},u)}$ is the random phase of the specular component, and $a_\ell^{(\tilde{u},u)}$ is the random complex coefficient of the ℓ-th scattered path. In addition, by definition, we also have $\mathrm{E}[\sum_\ell |a_\ell^{(\tilde{u},u)}|^2] = \frac{\Omega}{K+1}$.

Fig. 10 provides the results of s-FAMA under the multi-ray model when $K = 0$ and $N_p = 1000$. We highlight some discrepancies from our model as follows.

- For both channel models, the multiplexing gain begins to increase with U before it drops if U becomes too large for s-FAMA to resolve. The multiplexing gain is also

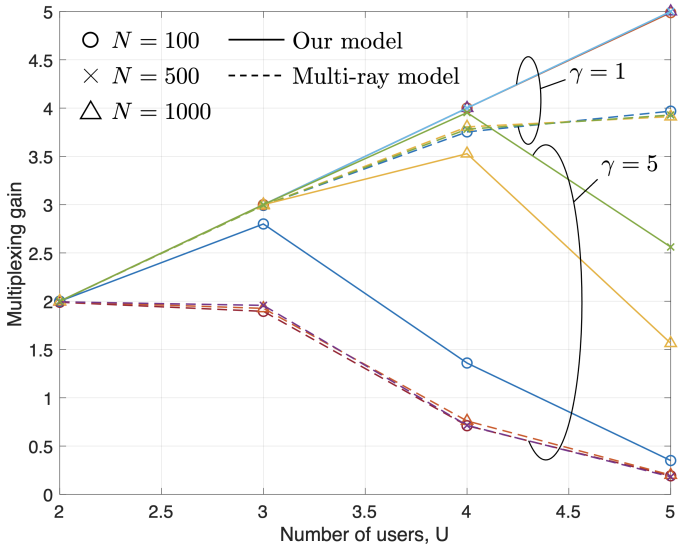

Fig. 10. The multiplexing gain performance for an U-user s-FAMA system using different channel models when the average SNR is set to $\Gamma = 20$dB, and $W = 5$. For the multi-ray model, we set $K = 0$ and $N_p = 1000$.

always upper bounded by the number of users, U, which can be achieved if the number of ports, N, and the size of the fluid antenna, W, are sufficiently large.

- In addition, the multiplexing gain for the generalized channel correlation model tends to be higher than that for the multi-ray channel. This suggests that the multi-ray model imposes stronger correlation between the channel ports than the generalized channel correlation model.
- It can also be observed that the number of ports, N, has more impact on the performance for the generalized channel correlation model than the multi-ray model.
- The results for both channel models are in agreement if the SINR threshold, γ, is not large, indicating that the analytical results derived from the generalized channel correlation model in this manuscript can be useful to understanding the performance of s-FAMA under the multi-ray model if γ is not large.

V. Conclusion

This paper has studied the performance of s-FAMA where a fluid antenna is equipped at each user to resolve the multiuser interference by switching its port only when the envelopes of the channels change, as opposed to f-FAMA where the ports are changed on a symbol-by-symbol basis. We derived exact expressions and bounds for the outage probability and multiplexing gain, and investigated how the achievable performance depends on the different system parameters such as the number of ports, the size of the antenna, the SIR threshold, and the number of users. The results have demonstrated that despite a weakened interference immunity compared to f-FAMA, the s-FAMA system can still effectively eliminate interference for multiple access if N is sufficiently large, while being a much more practically attractive approach.

Appendices

A. Proof of Theorem 1

To evaluate $\mathcal{I}$, we exploit an important connection between the generalized Marcum-Q function and confluent hypergeometric functions, first established in [25] and leveraged in [26] to obtain closed-form solutions to integrals of the type:

$$\mathrm{In}(\alpha_1, \alpha_2, \omega, p, \mu_1, \mu_2) \triangleq 2\int_0^\infty Q_{\mu_1}(\alpha_1 t, \alpha_2) t^{\mu_2} \exp(-pt^2) I_{\mu_2 - 1}(\omega t) dt. \quad (50)$$

Our aim is to rewrite $\mathcal{I}$ in terms of (50), for which closed-form solutions can be readily obtained by applying the results of [26]. The difference between $\mathcal{I}$ and (50) is that the integration variable appears in a different argument of the Marcum-Q function. However, we can exploit the known relationship of the generalized Marcum-Q function [25, (2)]

$$Q_m(a, b) = 1 - Q_{1-m}(b, a). \quad (51)$$

Using (51), we can rewrite $\mathcal{I}$ as

$$\begin{aligned}\mathcal{I} &= \int_0^\infty (1 - Q_0(\sqrt{\gamma}\beta, c)) \frac{\beta^M}{a^{M-1}} e^{-\frac{\beta^2 + a^2}{2}} I_{M-1}(a\beta) d\beta \\ &= \int_0^\infty \frac{\beta^M}{a^{M-1}} e^{-\frac{\beta^2 + a^2}{2}} I_{M-1}(a\beta) d\beta \\ &\quad - \int_0^\infty Q_0(\sqrt{\gamma}\beta, c) \frac{\beta^M}{a^{M-1}} e^{-\frac{\beta^2 + a^2}{2}} I_{M-1}(a\beta) d\beta. \quad (52)\end{aligned}$$

The first integral is recognized as $Q_M(a, 0) = 1$, according to the definition of the generalized Marcum-Q function [25, (1)], so that we have

$$\mathcal{I} = 1 - \frac{e^{-\frac{a^2}{2}}}{a^{M-1}} \int_0^\infty Q_0(\sqrt{\gamma}\beta, c) \beta^M e^{-\frac{\beta^2}{2}} I_{M-1}(a\beta) d\beta. \quad (53)$$

The remaining integral can be linked to (50), yielding

$$\mathcal{I} = 1 - \frac{e^{-\frac{a^2}{2}}}{2a^{M-1}} \mathrm{In}(\sqrt{\gamma}, c, a, 1/2, 0, M). \quad (54)$$

We can now apply [26, Proposition 1] to evaluate the integral $\mathrm{In}(\sqrt{\gamma}, c, a, 1/2, 0, M)$, which gives (55) (see top of next page). The integral $\mathrm{In}(\sqrt{\gamma}, c, a, 1/2, M, M)$ in (55) can also be evaluated as [26, Proposition 1]

$$\mathrm{In}(\sqrt{\gamma}, c, a, 1/2, M, M) = 2a^{M-1} e^{\frac{a^2}{2}} Q_M\left(a\sqrt{\frac{\gamma}{1+\gamma}}, c\sqrt{\frac{1}{1+\gamma}}\right). \quad (56)$$

Substituting (56) into (55) and simplifying terms, we finally arrive at (18) in which we have also used the fact that for the Pochhammer symbol, $(-x)_n = (-1)^n (x - n + 1)_n$.

B. Proof of Theorem 2

To prove the result, we need to work out the joint pdf of $X_1, X_2, \ldots, X_N$ and that of $Y_1, Y_2, \ldots, Y_N$. Given x_0 and y_0 (omitting the superscript (u, u) for conciseness) and defining

$$\mathcal{I} = 1 - \frac{e^{-\frac{a^2}{2}}}{2a^{M-1}} \left\{ \mathrm{In}(\sqrt{\gamma}, c, a, 1/2, M, M) - \frac{2}{a^{1-M}} \left(\frac{1}{1+\gamma}\right)^M \exp\left[\left(\frac{a^2}{2} - \frac{c^2}{2}\right)\left(\frac{1}{1+\gamma}\right)\right] \times \sum_{k=0}^{M-1} \sum_{j=0}^{M-k-1} \frac{(-1)^j(-M+k+1)_j}{j!} \left(\frac{c}{a}\right)^{j+k} (1+\gamma)^k (\sqrt{\gamma})^{j-k} I_{k+j}\left(\frac{ac\sqrt{\gamma}}{1+\gamma}\right) \right\} \quad (55)$$

$r_0 \triangleq x_0^2 + y_0^2$, X_k is a noncentral Chi-square random variable with two degrees of freedom and has the pdf [27, (2.12)]

$$p_{X_k|r_0}(x) = \frac{1}{2} e^{-\frac{x+\frac{\mu^2}{1-\mu^2} r_0}{2}} I_0\left(\sqrt{\frac{\mu^2}{1-\mu^2}\sqrt{r_0 x}}\right), \ x \geq 0, \quad (57)$$

where $I_0(\cdot)$ denotes the zero-order modified Bessel function of the first kind. As $\{X_k\}$ are all linked only by r_0, if r_0 is given and fixed, $\{X_k\}$ become independent. Hence, the joint pdf for $X_1, \ldots, X_N$ conditioned on r_0 is given by

$$p_{X_1,\ldots,X_N|r_0}(x_1, \ldots, x_N) = \prod_{k=1}^{N} \frac{1}{2} e^{-\frac{x_k+\frac{\mu^2}{1-\mu^2} r_0}{2}} I_0\left(\sqrt{\frac{\mu^2}{1-\mu^2}\sqrt{r_0 x_k}}\right). \quad (58)$$

Moreover, noting that r_0 is exponentially distributed with the pdf $p_{r_0}(r) = \frac{1}{2} e^{-\frac{r}{2}}$, we get the unconditioned joint pdf by

$$\begin{aligned} & p_{X_1,\ldots,X_N}(x_1, \ldots, x_N) \\ &= \int_0^\infty p_{r_0, X_1,\ldots,X_N}(r, x_1, \ldots, x_N) dr \\ &= \int_0^\infty \frac{e^{-\frac{r}{2}}}{2^{N+1}} \prod_{k=1}^{N} e^{-\frac{x_k+\frac{\mu^2}{1-\mu^2} r}{2}} I_0\left(\sqrt{\frac{\mu^2}{1-\mu^2}\sqrt{r x_k}}\right) dr. \end{aligned} \quad (59)$$

From (59), we can obtain the joint cumulative density function (cdf) of $X_1, \ldots, X_N$ by (60) (see top of next page). Note that (b) substitutes (59) into the cdf computation, (c) separates the integrands inside the product and writes the whole as a product of the integrals for $\{x_k\}$ and (d) recognizes that each integral over x_k is related to the cdf of a Rician random variable.[8]

Now, we denote $\tilde{r}_0 \triangleq \sum_{\tilde{u} \neq u} (x_0^{(\tilde{u},u)})^2 + (y_0^{(\tilde{u},u)})^2$ and then Y_k conditioned on $\tilde{r}_0$ is noncentral Chi-square distributed with $2(U-1)$ degrees of freedom and has the pdf [27, (2.12)]

$$p_{Y_k|\tilde{r}_0}(y) = \frac{1}{2} \left(\frac{y}{\frac{\mu^2}{1-\mu^2}\tilde{r}_0}\right)^{\frac{U-2}{2}} e^{-\frac{y+\frac{\mu^2}{1-\mu^2}\tilde{r}_0}{2}} \times I_{U-2}\left(\sqrt{\frac{\mu^2}{1-\mu^2}\sqrt{\tilde{r}_0 y}}\right). \quad (61)$$

Using the technique similar to that derives the joint pdf of $X_1, \ldots, X_N$, we can obtain the joint pdf of $Y_1, \ldots, Y_N$ as

$$\begin{aligned} & p_{Y_1,\ldots,Y_N}(y_1, \ldots, y_N) \\ &\overset{(a)}{=} \int_0^\infty p_{\tilde{r}_0}(\tilde{r}) p_{Y_1,\ldots,Y_N|\tilde{r}_0}(y_1, \ldots, y_N) d\tilde{r} \\ &\overset{(b)}{=} \int_0^\infty \underbrace{\frac{\tilde{r}^{U-2} e^{-\frac{\tilde{r}}{2}}}{2^{U-1}\Gamma(U-1)}}_{p_{\tilde{r}_0}(\tilde{r})} \prod_{k=1}^{N} \left[\frac{1}{2}\left(\frac{y_k}{\frac{\mu^2}{1-\mu^2}\tilde{r}}\right)^{\frac{U-2}{2}} \times e^{-\frac{y_k+\frac{\mu^2}{1-\mu^2}\tilde{r}}{2}} I_{U-2}\left(\sqrt{\frac{\mu^2}{1-\mu^2}\sqrt{\tilde{r} y_k}}\right)\right] d\tilde{r} \end{aligned} \quad (62)$$

in which (b) uses the fact that $\{Y_k\}$ are all independent when conditioned on $\tilde{r}_0$ and that $\tilde{r}_0$ has a Chi-square pdf with $2(U-1)$ degrees of freedom [27, (2.7)], and $\Gamma(n) = (n-1)!$.

With the above results, the outage probability, $\mathrm{Prob}(\mathrm{SIR} < \gamma)$, can be evaluated by (63) (see top of next page) in which (a) uses the results (60) and (62), (b) moves the integration over y_k inside the product, and (c) uses the fact that the total probability of a noncentral Chi-square random variable is one. Finally, the integral inside the product over y_k is recognized to be of the form (19) and consequently, applying the result in Corollary 1 by setting $b = \frac{\mu^2}{1-\mu^2}\tilde{r}$, $c = \frac{\mu\sqrt{\tilde{r}}}{\sqrt{1-\mu^2}}$ and $M = U-1$, we obtain the desired result (21) and complete the proof.

C. Proof of Corollary 2

From the definition

$$I_\nu(x) = \frac{1}{\pi} \int_0^\pi \cos(\nu\theta) e^{x\cos\theta} d\theta, \quad (64)$$

we can show (65) (see next page). Then substituting (65) into (21), we obtain (22) which completes the proof.

D. Proof of Theorem 3

Before we begin the proof, we have the following lemmas.

Lemma 1: We have the integral

$$\int_0^\infty t^{M-1} e^{-at} dt = a^{-M}(M-1)! = a^{-M}\Gamma(M). \quad (66)$$

Proof: The result (66) can be shown by repeatedly using integration by parts, which completes the proof. ■

Lemma 2: We have the integral

$$\int_0^\infty e^{-\frac{t}{2}} Q_M(b, a\sqrt{t}) dt = 2\left[1 - \left(\frac{a^2}{a^2+1}\right)^M e^{-\frac{b^2}{2(a^2+1)}}\right]. \quad (67)$$

[8] It is worth pointing out that this resembles the result in [10, Theorem 2] but the first port in [10] was used entirely as a reference port and hence the model there effectively has $N-1$ ports. Also, as mentioned in [18], the single spatial correlation parameter model used in this paper is more accurate.

$$
\begin{aligned}
F_{X_1,\ldots,X_N}(t_1,\ldots,t_N) &\overset{(a)}{=} \text{Prob}(X_1<t_1, X_2<t_2,\ldots,X_N<t_N)\\
&\overset{(b)}{=} \int_0^{\infty}\int_0^{t_N}\cdots\int_0^{t_1}\frac{e^{-\frac{r}{2}}}{2^{N+1}}\prod_{k=1}^{N} e^{-\frac{x_k+\frac{\mu^2}{1-\mu^2}r}{2}} I_0\left(\sqrt{\frac{\mu^2}{1-\mu^2}}\sqrt{rx_k}\right)dx_1\cdots dx_N dr\\
&\overset{(c)}{=} \int_0^{\infty}\frac{1}{2}e^{-\frac{r}{2}}\left[\prod_{k=1}^{N}\int_0^{t_k}\frac{1}{2}e^{-\frac{x_k+\frac{\mu^2}{1-\mu^2}r}{2}} I_0\left(\sqrt{\frac{\mu^2}{1-\mu^2}}\sqrt{rx_k}\right)dx_k\right]dr\\
&\overset{(d)}{=} \int_0^{\infty}\frac{1}{2}e^{-\frac{r}{2}}\prod_{k=1}^{N}\left[1-Q_1\left(\sqrt{\frac{\mu^2}{1-\mu^2}}\sqrt{r},\sqrt{t_k}\right)\right]dr
\end{aligned}
\tag{60}
$$

$$
\begin{aligned}
&\text{Prob}\left(\frac{X_1}{Y_1}<\gamma,\frac{X_2}{Y_2}<\gamma,\ldots,\frac{X_N}{Y_N}<\gamma\right)\\
&=\int_0^{\infty}\cdots\int_0^{\infty}F_{X_1,\ldots,X_N|Y_1,\ldots,Y_N}(\gamma y_1,\ldots,\gamma y_N)p_{Y_1,\ldots,Y_N}(y_1,\ldots,y_N)dy_1\cdots dy_N\\
&\overset{(a)}{=}\underbrace{\int_0^{\infty}\cdots\int_0^{\infty}}_{y_1\cdots y_N}\int_{r=0}^{\infty}\frac{1}{2}e^{-\frac{r}{2}}\prod_{k=1}^{N}\left[1-Q_1\left(\sqrt{\frac{\mu^2}{1-\mu^2}}\sqrt{r},\sqrt{\gamma y_k}\right)\right]dr\times\\
&\qquad\int_{\tilde{r}=0}^{\infty}\frac{\tilde{r}^{U-2}e^{-\frac{\tilde{r}}{2}}}{2^{U-1}\Gamma(U-1)}\prod_{k=1}^{N}\left[\frac{1}{2}\left(\frac{y_k}{\frac{\mu^2}{1-\mu^2}\tilde{r}}\right)^{\frac{U-2}{2}}e^{-\frac{y_k+\frac{\mu^2}{1-\mu^2}\tilde{r}}{2}}I_{U-2}\left(\sqrt{\frac{\mu^2}{1-\mu^2}}\sqrt{\tilde{r}y_k}\right)\right]d\tilde{r}dy_1\cdots dy_N\\
&\overset{(b)}{=}\int_0^{\infty}\int_0^{\infty}\frac{\tilde{r}^{U-2}e^{-\frac{r+\tilde{r}}{2}}}{2^{U-1}\Gamma(U-1)}\prod_{k=1}^{N}\int_{y_k=0}^{\infty}\left[1-Q_1\left(\sqrt{\frac{\mu^2}{1-\mu^2}}\sqrt{r},\sqrt{\gamma y_k}\right)\right]\times\\
&\qquad\frac{1}{2}\left(\frac{y_k}{\frac{\mu^2}{1-\mu^2}\tilde{r}}\right)^{\frac{U-2}{2}}e^{-\frac{y_k+\frac{\mu^2}{1-\mu^2}\tilde{r}}{2}}I_{U-2}\left(\sqrt{\frac{\mu^2}{1-\mu^2}}\sqrt{\tilde{r}y_k}\right)dy_k dr d\tilde{r}\\
&\overset{(c)}{=}\int_0^{\infty}\int_0^{\infty}\frac{\tilde{r}^{U-2}e^{-\frac{r+\tilde{r}}{2}}}{2^{U-1}\Gamma(U-1)}\prod_{k=1}^{N}\left[1-\int_{y_k=0}^{\infty}Q_1\left(\sqrt{\frac{\mu^2}{1-\mu^2}}\sqrt{r},\sqrt{\gamma y_k}\right)\times\right.\\
&\qquad\left.\frac{1}{2}\left(\frac{y_k}{\frac{\mu^2}{1-\mu^2}\tilde{r}}\right)^{\frac{U-2}{2}}e^{-\frac{y_k+\frac{\mu^2}{1-\mu^2}\tilde{r}}{2}}I_{U-2}\left(\sqrt{\frac{\mu^2}{1-\mu^2}}\sqrt{\tilde{r}y_k}\right)dy_k\right]dr d\tilde{r}
\end{aligned}
\tag{63}
$$

Proof: Substituting $p=1$ and $c=0$ in [28, (B.54)], we have

$$\int_0^{\infty}xe^{-\frac{x^2}{2}}Q_M(b,ax)dx=1-\left(\frac{a^2}{a^2+1}\right)^M e^{-\frac{b^2}{2(a^2+1)}}. \tag{68}$$

Now, changing the variable $t=x^2$, we get

$$\int_0^{\infty}xe^{-\frac{x^2}{2}}Q_M(b,ax)dx=\frac{1}{2}\int_0^{\infty}e^{-\frac{t}{2}}Q_M(b,a\sqrt{t})dt. \tag{69}$$

Equalling (68) and (69) then obtains the required result. ■

Take the outage probability in (21) and write it in the form

$$\text{Prob}(\text{SIR}<\gamma)=\int_0^{\infty}\int_0^{\infty}\frac{\tilde{r}^{U-2}}{2^U\Gamma(U-1)}e^{-\frac{r+\tilde{r}}{2}}\times\left[1-\underbrace{(1-Q_{U-1}(\cdot,\cdot)+\cdots)}_{Z}\right]^N drd\tilde{r}. \tag{70}$$

Apparently, the outage probability is a decreasing function of N and hence $Z<1$. Typically, N needs to be large to bring down the outage probability to an acceptable level given the multiple interferers, which implies that Z is very small. Thus, it is possible to approximate the outage probability by

$$\text{Prob}(\text{SIR}<\gamma)\approx\int_0^{\infty}\int_0^{\infty}\frac{\tilde{r}^{U-2}}{2^U\Gamma(U-1)}e^{-\frac{r+\tilde{r}}{2}}\times\left[1-N\underbrace{(1-Q_{U-1}(\cdot,\cdot)+\cdots)}_{Z}\right]drd\tilde{r}. \tag{71}$$

Now, using the lower bound [29]

$$I_{\nu}(z)>\frac{1}{\Gamma(\nu+1)}\left(\frac{z}{2}\right)^{\nu}, \tag{72}$$

we can obtain (73) (see top of next page) where (a) also uses the approximation that $\gamma+1\approx\gamma$ for large γ. Using (71) and (73), we get the upper bound of the outage probability

$$\text{Prob}(\text{SIR}<\gamma)<(1-N)A+NB-NC, \tag{74}$$

$$e^{-\frac{\mu^2}{2(1-\mu^2)}\left(\frac{\gamma\tilde{r}+r}{\gamma+1}\right)} I_{k+j}\left(\frac{\mu^2}{1-\mu^2}\frac{\sqrt{\gamma\tilde{r}r}}{\gamma+1}\right) = \frac{1}{\pi}\int_0^\pi \cos((k+j)\theta) e^{-\frac{\mu^2}{2(1-\mu^2)}\frac{1}{\gamma+1}\left[\gamma\tilde{r}+r-2\sqrt{\gamma\tilde{r}r}\cos\theta\right]} d\theta$$
$$= \frac{1}{\pi}\int_0^\pi \cos((k+j)\theta) e^{-\frac{\mu^2}{2(1-\mu^2)}\frac{1}{\gamma+1}\left[(\sqrt{\gamma\tilde{r}}-\sqrt{r})^2+2\sqrt{\gamma\tilde{r}r}(1-\cos\theta)\right]} d\theta$$
$$= \frac{1}{\pi} e^{-\frac{\mu^2}{2(1-\mu^2)}\frac{1}{\gamma+1}(\sqrt{\gamma\tilde{r}}-\sqrt{r})^2} \int_0^\pi \cos((k+j)\theta) e^{-\frac{\mu^2}{(1-\mu^2)}\frac{1}{\gamma+1}\sqrt{\gamma\tilde{r}r}(1-\cos\theta)} d\theta \quad (65)$$

$$\left(\frac{1}{\gamma+1}\right)^{U-1} e^{-\frac{\mu^2}{2(1-\mu^2)}\frac{\gamma\tilde{r}+r}{\gamma+1}} \sum_{k,j} \frac{(U-1-(k+j))_j}{j!} \left(\frac{\sqrt{r}}{\sqrt{\tilde{r}}}\right)^{j+k} \gamma^{\frac{j+k}{2}} I_{k+j}\left(\frac{\mu^2}{1-\mu^2}\frac{\sqrt{\gamma r\tilde{r}}}{\gamma+1}\right)$$
$$\overset{(a)}{>} e^{-\frac{\mu^2}{2(1-\mu^2)}\frac{\gamma\tilde{r}+r}{\gamma+1}} \sum_{k,j} \frac{(U-1-(k+j))_j}{j!} \left(\frac{\sqrt{r}}{\sqrt{\tilde{r}}}\right)^{j+k} \frac{1}{\gamma^{U-1-\frac{k+j}{2}}} \frac{1}{\Gamma(k+j+1)} \left[\frac{\mu^2}{2(1-\mu^2)}\frac{\sqrt{\gamma r\tilde{r}}}{\gamma+1}\right]^{k+j}$$
$$\overset{(b)}{=} e^{-\left[\frac{\mu^2}{2(1-\mu^2)}\frac{\gamma}{\gamma+1}\right]\tilde{r}} \sum_{k,j} \frac{(U-1-(k+j))_j}{(k+j)!j!} \frac{1}{\gamma^{U-1-\frac{k+j}{2}}} \left[\frac{\mu^2}{2(1-\mu^2)}\frac{\sqrt{\gamma}}{\gamma+1}\right]^{k+j} e^{-\left[\frac{\mu^2}{2(1-\mu^2)}\frac{1}{\gamma+1}\right]r} r^{k+j} \quad (73)$$

where

$$A = \int_0^\infty \int_0^\infty \frac{\tilde{r}^{U-2}}{2^U\Gamma(U-1)} e^{-\frac{r+\tilde{r}}{2}} dr d\tilde{r}, \quad (75)$$

$$B = \int_0^\infty \int_0^\infty \frac{\tilde{r}^{U-2}}{2^U\Gamma(U-1)} e^{-\frac{r+\tilde{r}}{2}} \times Q_{U-1}\left(\frac{\mu\sqrt{\gamma}\sqrt{\tilde{r}}}{\sqrt{1-\mu^2}\sqrt{\gamma+1}}, \frac{\mu\sqrt{r}}{\sqrt{1-\mu^2}\sqrt{\gamma+1}}\right) dr d\tilde{r}, \quad (76)$$

and C is given by (77) (see next page).

To evaluate A, we separate the integrals over r and $\tilde{r}$ and apply Lemma 1 to express the integral over $\tilde{r}$, which gives

$$A = \frac{1}{2^U\Gamma(U-1)} \times 2^{U-1}\Gamma(U-1) \times 2 = 1. \quad (78)$$

For B, we first evaluate the inner integral over r using Lemma 2 by setting $b = \frac{\mu}{\sqrt{1-\mu^2}}\sqrt{\frac{\gamma}{\gamma+1}}\sqrt{\tilde{r}}$ and $a = \frac{\mu}{\sqrt{1-\mu^2}}\frac{1}{\sqrt{\gamma+1}}$ and after some simplifications, we then get

$$B = \frac{1}{2^{U-1}\Gamma(U-1)} \int_0^\infty \tilde{r}^{U-2} e^{-\frac{\tilde{r}}{2}} d\tilde{r} - \frac{1}{2^{U-1}\Gamma(U-1)} \left(\frac{\frac{\mu^2}{1-\mu^2}\frac{1}{\gamma+1}}{\frac{\mu^2}{1-\mu^2}\frac{1}{\gamma+1}+1}\right)^{U-1} \times \int_0^\infty \tilde{r}^{U-2} e^{-\frac{1}{2}\left[1+\frac{\frac{\mu^2}{1-\mu^2}\frac{\gamma}{\gamma+1}}{\frac{\mu^2}{1-\mu^2}\frac{1}{\gamma+1}+1}\right]\tilde{r}} d\tilde{r}. \quad (79)$$

By applying Lemma 1 to compute the first and second terms of the above, it can be shown that

$$B = 1 - \left(\frac{\mu^2}{\gamma+1}\right)^{U-1}. \quad (80)$$

Now, we derive a closed-form expression for C as (81) (see top of next page) where (a) expresses the integral as the product of two integrals, one over r and another one over $\tilde{r}$, (b) applies the result of Lemma 1 to evaluate the two integrals, (c) makes some simplifications, (d) considers, for large γ and small μ, that $1+(1-\mu^2)\gamma \approx (1-\mu^2)\gamma$, $1+\gamma \approx \gamma$ and $1-\mu^2+\gamma \approx \gamma$, (e) tidies up the expression and (f) ignores the higher-order terms which get smaller, to obtain the final expression.

As a result, the upper bound can be found as

$$\text{Prob}(\text{SIR} < \gamma) < (1-N)(1) + N\left[1-\left(\frac{\mu^2}{\gamma+1}\right)^{U-1}\right] - N\left(\frac{1-\mu^2}{\gamma}\right)^{U-1} = 1 - N\left(\frac{\mu^2}{\gamma+1}\right)^{U-1} - N\left(\frac{1-\mu^2}{\gamma}\right)^{U-1}. \quad (82)$$

Finally, note that we have used the linearization $(1-Z)^N \approx 1-NZ$ for small Z and therefore, the upper bound (82) can become negative when N is extremely large. As a result, the operation $(\cdot)^+$ is adopted to guarantee positivity of the upper bound, resulting in the expression (23). Then, for small μ, we have $(\mu^2)^{U-1} \ll (1-\mu^2)^{U-1}$ and thus (24) is obtained. Lastly, if $W \geq 1$, then according to (8), we can substitute $\mu^2 = \frac{1}{\pi W}$ into (24), to obtain the expression (25).

Overall, it can be recognized that (25) is a result of a number of approximations. Most notably, the approximations rely on having a large γ and small μ in (d) and (f) of (81). To have a small μ, it means that W should not be small. In addition, the accuracy also depends on the tightness of the bound (72). For finite r and $\tilde{r}$, the bound is tight if again μ is small while if r and $\tilde{r}$ are infinitely large, the corresponding term in Z, or the left hand side of (73), will approach 0. In summary, the result (25) should be more accurate for larger γ and W.

REFERENCES

[1] F. Tariq *et al.*, "A speculative study on 6G," *IEEE Wireless Commun.*, vol. 27, no. 4, pp. 118–125, Aug. 2020.

[2] E. G. Larsson, O. Edfors, F. Tufvesson, and T. L. Marzetta, "Massive MIMO for next generation wireless systems," *IEEE Commun. Mag.*, vol. 52, no. 2, pp. 186–195, Feb. 2014.

$$C=\int_0^{\infty}\int_0^{\infty}\frac{\tilde{r}^{U-2}}{2^U\Gamma(U-1)}e^{-\frac{r+\tilde{r}}{2}}e^{-\left[\frac{\mu^2}{2(1-\mu^2)}\frac{\gamma}{\gamma+1}\right]\tilde{r}}\times \sum_{k,j}\frac{(U-1-(k+j))_j}{(k+j)!j!}\frac{1}{\gamma^{U-1-\frac{k+j}{2}}}\left[\frac{\mu^2}{2(1-\mu^2)}\frac{\sqrt{\gamma}}{\gamma+1}\right]^{k+j}e^{-\left[\frac{\mu^2}{2(1-\mu^2)}\frac{1}{\gamma+1}\right]r}r^{k+j}drd\tilde{r} \quad (77)$$

$$\begin{aligned}
C &\overset{(a)}{=} \int_0^{\infty}\frac{\tilde{r}^{U-2}e^{-\frac{1}{2}\left[1+\frac{\mu^2}{1-\mu^2}\frac{\gamma}{\gamma+1}\right]\tilde{r}}}{2^U\Gamma(U-1)}d\tilde{r}\times \sum_{k,j}\frac{(U-1-(k+j))_j}{(k+j)!j!}\frac{1}{\gamma^{U-1-\frac{k+j}{2}}}\left[\frac{\mu^2}{2(1-\mu^2)}\frac{\sqrt{\gamma}}{\gamma+1}\right]^{k+j}\int_0^{\infty}e^{-\frac{1}{2}\left[1+\frac{\mu^2}{1-\mu^2}\frac{1}{\gamma+1}\right]r}r^{k+j}dr \\
&\overset{(b)}{=} \frac{1}{2}\left[1+\frac{\mu^2}{1-\mu^2}\frac{\gamma}{\gamma+1}\right]^{-(U-1)}\sum_{k,j}\frac{(U-1-(k+j))_j}{(k+j)!j!}\frac{1}{\gamma^{U-1-\frac{k+j}{2}}}\left[\frac{\mu^2}{2(1-\mu^2)}\frac{\sqrt{\gamma}}{\gamma+1}\right]^{k+j}\times \left[\frac{1}{2}\left(1+\frac{\mu^2}{1-\mu^2}\frac{1}{\gamma+1}\right)\right]^{-(k+j+1)}\Gamma(k+j+1) \\
&\overset{(c)}{=} \sum_{k,j}\frac{(U-1-(k+j))_j}{j!\,\gamma^{U-1-(k+j)}}\frac{\left(\mu^2\right)^{k+j}}{\left[1+(1-\mu^2)\gamma\right]^{k+j+1}}\frac{\left[(1-\mu^2)(1+\gamma)\right]^U}{(1-\mu^2+\gamma)^{U-1}} \\
&\overset{(d)}{\approx} \sum_{k,j}\frac{(U-1-(k+j))_j}{j!}\frac{1}{\gamma^{U-1-(k+j)}}\frac{\left(\mu^2\right)^{k+j}}{\left[(1-\mu^2)\gamma\right]^{k+j+1}}\frac{\left[(1-\mu^2)\gamma\right]^U}{(\gamma)^{U-1}} \\
&\overset{(e)}{=} \left(\frac{1-\mu^2}{\gamma}\right)^{U-1}\sum_{k,j}\frac{(U-1-(k+j))_j}{j!}\left(\frac{\mu^2}{1-\mu^2}\right)^{k+j}\overset{(f)}{\approx}\left(\frac{1-\mu^2}{\gamma}\right)^{U-1}
\end{aligned} \quad (81)$$

[3] N. Ye, J. An and J. Yu, "Deep-learning-enhanced NOMA transceiver design for massive MTC: Challenges, state of the art, and future directions," *IEEE Wireless Commun.*, vol. 28, no. 4, pp. 66–73, Aug. 2021.

[4] K. K. Wong and K. F. Tong, "Fluid antenna multiple access," *IEEE Trans. Wireless Commun.*, vol. 21, no. 7, pp. 4801–4815, Jul. 2022.

[5] K. N. Paracha, A. D. Butt, A. S. Alghamdi, S. A. Babale, and P. J. Soh, "Liquid metal antennas: Materials, fabrication and applications," *Sensors 2020*, 20, 177.

[6] Y. Huang, L. Xing, C. Song, S. Wang and F. Elhouni, "Liquid antennas: Past, present and future," *IEEE Open J. Antennas and Propag.*, vol. 2, pp. 473–487, 2021.

[7] B. A. Cetiner, H. Jafarkhani, Jiang-Yuan Qian, Hui Jae Yoo, A. Grau and F. De Flaviis, "Multifunctional reconfigurable MEMS integrated antennas for adaptive MIMO systems," *IEEE Commun. Mag.*, vol. 42, no. 12, pp. 62–70, Dec. 2004.

[8] A. Grau Besoli and F. De Flaviis, "A multifunctional reconfigurable pixeled antenna using MEMS technology on printed circuit board," *IEEE Trans. Antennas & Propag.*, vol. 59, no. 12, pp. 4413–4424, Dec. 2011.

[9] S. Song and R. D. Murch, "An efficient approach for optimizing frequency reconfigurable pixel antennas using genetic algorithms," *IEEE Trans. Antennas & Propag.*, vol. 62, no. 2, pp. 609–620, Feb. 2014.

[10] K. K. Wong, A. Shojaeifard, K.-F. Tong and Y. Zhang, "Fluid antenna systems," *IEEE Trans. Wireless Commun.*, vol. 20, no. 3, pp. 1950–1962, Mar. 2021.

[11] K. K. Wong, A. Shojaeifard, K.-F. Tong and Y. Zhang, "Performance limits of fluid antenna systems," *IEEE Commun. Letters*, vol. 24, no. 11, pp. 2469–2472, Nov. 2020.

[12] Z. Chai, K. K. Wong, K. F. Tong, Y. Chen and Y. Zhang, "Port selection for fluid antenna systems," *IEEE Commun. Letters*, vol. 26, no. 5, pp. 1180–1184, May 2022.

[13] L. Tlebaldiyeva, G. Nauryzbayev, S. Arzykulov, A. Eltawil and T. Tsiftsis, "Enhancing QoS through fluid antenna systems over correlated Nakagami-m fading channels," in *Proc. IEEE Wireless Commun. Netw. Conf. (WCNC)*, pp. 78–83, 10-13 Apr. 2022, Austin, TX, USA.

[14] M. Khammassi, A. Kammoun, and M.-S. Alouini, "A new analytical approximation of the fluid antenna system channel," [Online] arXiv preprint arXiv:2203.09318, 2022.

[15] C. Psomas, G. M. Kraidy, K. K. Wong, and I. Krikidis, "On the diversity and coded modulation design of fluid antenna systems," [Online] arXiv preprint arXiv:2205.01962, 2022.

[16] P. Mukherjee, C. Psomas, and I. Krikidis, "On the level crossing rate of fluid antenna systems," [Online] arXiv preprint arXiv:2205.01711, 2022.

[17] K. K. Wong, K. F. Tong, Y. Shen, Y. Chen, and Y. Zhang, "Bruce Lee-inspired fluid antenna system: Six research topics and the potentials for 6G," *Frontiers Commun. and Netw., section Wireless Commun.*, 3:853416, Mar. 2022.

[18] K. K. Wong, K. F. Tong, Y. Chen and Y. Zhang, "Closed-form expressions for spatial correlation parameters for performance analysis of fluid antenna systems," *IET Electronics Letters*, vol. 58, no. 11, pp. 454–457, Apr. 2022.

[19] K. K. Wong, K. F. Tong, Y. Chen, and Y. Zhang, "Fast fluid antenna multiple access enabling massive connectivity," *IEEE Commun. Letters*, vol. 27, no. 2, pp. 711–715, Feb. 2023.

[20] K. K. Wong, K. F. Tong, Y. Chen, and Y. Zhang, "Extra-large MIMO enabling slow fluid antenna massive access for millimeter-wave bands," *IET Elect. Letters*, vol. 58, no. 25, pp. 1016–1018, Dec. 2022.

[21] N. Waqar, K. K. Wong, K. F. Tong, A. Sharples, and Y. Zhang, "Deep learning enabled slow fluid antenna multiple access," to appear in *IEEE Commun. Letters*, 2023.

[22] N. C. Beaulieu, K. T. Hemachandra, "Novel simple representations for Gaussian class multivariate distributions with generalized correlation," *IEEE Trans. Inform. Theory*, vol. 57, no. 12, pp. 8072–8083, 2011.

[23] T. S. Rappaport, G. R. MacCartney, M. K. Samimi, and S. Sun, "Wideband millimeter-wave propagation measurements and channel models for future wireless communication system design," *IEEE Trans. Commun.*, vol. 63, no. 9, pp. 3029–3056, 2015.

[24] I. A. Hemadeh, K. Satyanarayana, M. El-Hajjar, and L. Hanzo, "Millimeter-wave communications: Physical channel models, design considerations, antenna constructions, and link-budget," *IEEE Commun. Surv. Tutor.*, vol. 20, no. 2, pp. 870–913, 2018.

[25] D. Morales-Jimenez, F. J. Lopez-Martinez, E. Martos-Naya, J. F. Paris, A. Lozano, "Connections between the generalized Marcum Q-function and a class of hypergeometric functions," *IEEE Trans. Inform. Theory*, vol. 60, no. 2, pp. 1077–1082, Feb. 2014.

[26] N. Y. Ermolova and O. Tirkkonen. "Laplace transform of product of generalized Marcum Q, Bessel I, and power functions with applications," *IEEE Trans. Signal Proc.*, vol. 62, no. 11, pp. 2938–2944, Jun. 2014.
[27] S. M. Kay, *Fundamentals of Statistical Signal Processing: Detection Theory*, Pearson Education, 1998.
[28] M. K. Simon, *Probability Distributions Involving Gaussian Random Variables: A Handbook for Engineers and Scientists*, Springer, Boston, MA, 2002.
[29] Y. L. Luke, "Inequalities for generalized hypergeometric functions," *J. Approx. Theory*, vol. 5, no. 1, pp. 41–65, Jan. 1972.

(Kit) Kai-Kit Wong (M'01-SM'08-F'16) received the BEng, the MPhil, and the PhD degrees, all in Electrical and Electronic Engineering, from the Hong Kong University of Science and Technology, Hong Kong, in 1996, 1998, and 2001, respectively. After graduation, he took up academic and research positions at the University of Hong Kong, Lucent Technologies, Bell-Labs, Holmdel, the Smart Antennas Research Group of Stanford University, and the University of Hull, UK. He is Chair in Wireless Communications at the Department of Electronic and Electrical Engineering, University College London, UK.

His current research centers around 5G and beyond mobile communications. He is a co-recipient of the 2013 IEEE Signal Processing Letters Best Paper Award and the 2000 IEEE VTS Japan Chapter Award at the IEEE Vehicular Technology Conference in Japan in 2000, and a few other international best paper awards. He is Fellow of IEEE and IET and is also on the editorial board of several international journals. He is the Editor-in-Chief for IEEE Wireless Communications Letters since 2020.

David Morales-Jimenez (M'13-SM'19) is an RyC Research Professor with the Department of Signal Theory, Networking and Communications at University of Granada (Spain). He received the M.Sc. and Ph.D. degrees in Telecommunication Technologies from University of Malaga (Spain) in 2008 and 2011, respectively. Between 2011 and 2013 he was a Postdoctoral Fellow at Universitat Pompeu Fabra (Barcelona, Spain). He then joined the Hong Kong University of Science and Technology (HKUST), first as Visiting Scholar (2014-2016) and then as Research Assistant Professor (2016-2018) with the Department of Electronic and Computer Engineering. He was a Lecturer (Assistant Professor) at Queen?s University Belfast (2018-2021) and an Associate Professor at University of Malaga (2021-2022). He also held visiting appointments at University College London (Electronic and Electrical Engineering, 2010) and at Stanford University (Statistics Department, 2015). His research interests include statistical signal processing, random matrix theory, and high-dimensional statistics, with multidisciplinary applications to wireless communications and computational biology.

Prof. Morales is an Associate Editor of the IEEE Transactions on Signal Processing and an Elected Member of the IEEE Technical Committee on Signal Processing for Communications and Networking (SPCOM). He received the Best Ph.D. Thesis Award in Electrical and Computer Engineering by the University of Malaga. He and his coauthors received the Best 'Statistica Sinica' paper award at Joint Statistical Meetings 2020. He was a Poster Co-Chair of the IEEE Communication Theory Workshop 2022 and a General Co-Chair of the IEEE Spanish Workshop on Signal Processing, Information Theory and Communications 2022.

Kin Fai Tong (M'99-SM'13-F'23) received the B.Eng. and Ph.D. degrees in electronic engineering from the City University of Hong Kong in 1993 and 1997, respectively. After graduation, Dr. Tong worked in the Department of Electronic Engineering at City University of Hong Kong as a Research Fellow. Two years later, he took up the post Expert researcher in the Photonic Information Technology Group and Millimetre-wave Devices Group at the National Institute of Information and Communications Technology (NiCT), Japan, where his main research focused on photonic-millimeter-wave planar antennas at 10GHz, 38 GHz and 60 GHz for high-speed wireless communications systems. In 2005, he started his academic career in the Department of Electronic and Electrical Engineering, UCL, as a lecturer. Now Dr. Tong is Chair in Antennas, Microwave and Millimeter-wave Engineering in the department. His current research interests include millimeter-wave and THz antennas, fluid antennas, 3D printed antennas and sub-GHz long range IoT networks. He served as the General Co-Chair of the 2017 International Workshop on Electromagnetics (iWEM), and Lead Guest Editor of IEEE OJAP in 2020.

Chan-Byoung Chae (Fellow, IEEE) received the Ph.D. degree in electrical and computer engineering from The University of Texas at Austin (UT) in 2008.

Prior to joining UT, he was a Research Engineer at the Telecommunications Research and Development Center, Samsung Electronics, Suwon, South Korea, from 2001 to 2005. He is currently an Underwood Distinguished Professor with the School of Integrated Technology, Yonsei University, South Korea. Before joining Yonsei University, he was with Bell Labs, Alcatel-Lucent, Murray Hill, NJ, USA, from 2009 to 2011, as a Member of Technical Staff, and Harvard University, Cambridge, MA, USA, from 2008 to 2009, as a Post-Doctoral Research Fellow.

Dr. Chae was a recipient/co-recipient of the CES Innovation Award in 2023, the IEEE ICC Best Demo Award in 2022, the IEEE WCNC Best Demo Award in 2020, the Best Young Engineer Award from the National Academy of Engineering of Korea (NAEK) in 2019, the IEEE DySPAN Best Demo Award in 2018, the IEEE/KICS Journal of Communications and Networks Best Paper Award in 2018, the IEEE INFOCOM Best Demo Award in 2015, the IEIE/IEEE Joint Award for Young IT Engineer of the Year in 2014, the KICS Haedong Young Scholar Award in 2013, the *IEEE Signal Processing Magazine* Best Paper Award in 2013, the IEEE ComSoc AP Outstanding Young Researcher Award in 2012, and the IEEE VTS Dan. E. Noble Fellowship Award in 2008. He is currently the Editor-in-Chief of the IEEE TRANSACTIONS ON MOLECULAR, BIOLOGICAL, AND MULTI-SCALE COMMUNICATIONS and a Senior Editor of the IEEE WIRELESS COMMUNICATIONS LETTERS. He has served/serves as an Editor for the *IEEE Communications Magazine* since 2016, the IEEE TRANSACTIONS ON WIRELESS COMMUNICATIONS from 2012 to 2017, and the IEEE WIRELESS COMMUNICATIONS LETTERS since 2016. He is an IEEE ComSoc Distinguished Lecturer from 2020 to 2023. He is an IEEE Fellow and NAEK Fellow.